Inorganic Chemistry

Article

pubs.acs.org/IC

Nonclassic Metallointercalators with Dipyridophenazine: DNA Interaction Studies and Leishmanicidal Activity

João Madureira,*[,†,‡,§] Catarina I. V. Ramos,[‖] Mónica Marques,[⊥] Carla Maia,[⊥,#] Bruno de Sousa,[⊥,#,&] Lenea Campino,[⊥,%] M. Graça Santana-Marques,[‖] and Nicholas Farrell*[,†]

[†]Department of Chemistry, Virginia Commonwealth University, 1001 West Main Street, Richmond, Virginia 23284, United States

[‡]Departamento de Química e Bioquímica, Universidade de Lisboa, Campo Grande, 1749-016 Lisboa, Portugal

[‖]Departamento de Química, Universidade de Aveiro, Campus de Santiago, 3810-193 Aveiro, Portugal

[⊥]Unidade de Parasitologia Médica, [#]Centro de Malária e outras Doenças Tropicais, and [&]Unidade de Saúde Pública Internacional e Bioestatística, Instituto Instituto de Higiene e Medicina Tropical (IHMT), Universidade Nova de Lisboa (UNL), Rua da Junqueira 100, 1349-008 Lisboa, Portugal

[%]Departamento Ciências Biomédicas e Medicina, Universidade do Algarve, Campus de Gambelas, 8000-117 Faro, Portugal

Supporting Information

ABSTRACT: Complexes $[Cu(CH_3COO)(dppz)_2]CH_3COO$ (**1**) and $[Zn(dppz)_2](BF_4)_2$ (**2**) with the intercalator dipyridophenazine (dppz) were prepared to obtain metallointercalators with increased geometrical flexibility compared to octahedral ones. Biophysical results (thermal denaturation, circular dichroism, rheometry, atomic force microscopy) indicate a strong interaction with DNA by intercalation and the existence of a positive cooperative effect with groove binding being preferred at low concentration of complexes. Induced circular dichroism (ICD) studies with DNA show that compounds **1** and **2** have a preferred orientation when binding to DNA. Since the compounds lack functional groups to permit hydrogen bonds, a combined intercalation/covalent binding mode is plausible. Further studies by QTof-ESI-MS and tandem experiments with GC oligonucleotides strongly support this dual-binding mode, since binding requires loss of one dppz unit with the copper center remaining attached to DNA even after another dppz loss. DNA saturation by the copper compound occurs at about one-half the concentration required for the zinc complex. Molecular modeling results suggest that it is caused by the increased ability of Cu(II) to distort to a more planar structure during interaction with DNA. Compounds **1** and **2** are active against a viscerotropic *Leishmania infantum* strain at submicromolar concentrations (IC_{50} = 0.57 and 0.46 μM, respectively), being more active than the reference drug miltefosine (M) (15.97 μM). They are also more cytotoxic than the control on human macrophages (MTD_{25} = 0.41 (**1**), 0.63 (**2**)). Besides miltefosine, the zinc compound is the only one with a MTD_{25}/IC_{50} ratio above 1 on the promastigote phase (1.39) and was further studied on the amastigote form with a significant improvement in the therapeutic index (2.51). Combined analysis of DNA biophysical studies, parasite activity, and cytotoxicity measurements suggests that intercalation correlates with leishmanicidal activity, while cytotoxicity results are justified by a combination of DNA intercalation and possible radical formation in the case of Cu(II), most probably hydroxyl and/or singlet oxygen radicals.

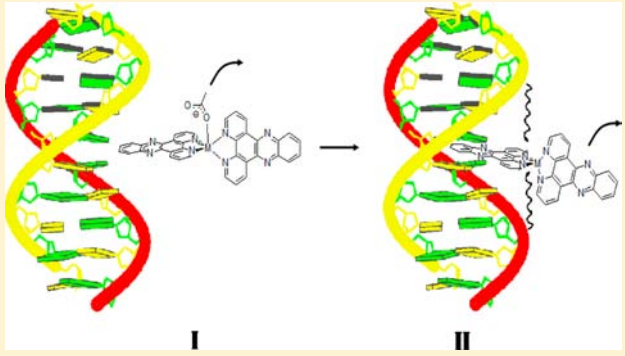

1. INTRODUCTION

The classical approach to inorganic drug design of DNA binders has been mainly centered on compounds able to form covalent bonds with nucleobases or intercalate between base pairs. The former group has among their more representative examples Pt(II) drugs, typically with one or more labile ligands to induce hydrolysis and permit DNA coordination.[1] The latter group is characterized by inert coordinatively saturated square-planar and octahedral complexes with ligands with extended aromatic surfaces,[2] more commonly from Pt(II), Rh(II/II), Ru(II), and Os(II).

While less studied, combination of these two characteristics, with development of dual-binding mode complexes, has been gaining relevance since the late 1980s. Typical covalent compounds of Pt(II) were modified to introduce an intercalator directly bound to the metal or with a linker between the metal center and the intercalator (side arms).[3] Similarly, Ru(II) compounds, with a π-bond organometallic fragment like $[RuCl(\eta^6\text{-arene})(en)]^+$ or similar ones, have also been explored by Sadler and co-workers.[4] Alternatively,

Received: April 29, 2013
Published: July 11, 2013

polynuclear complexes with dissimilar units, each one binding DNA by different mechanisms (covalent vs intercalation), may be assembled with linker bridges.[5,6] The dual-binding mode approach has resulted in drugs with enhanced cytotoxicity,[7,8] decreased cross-resistance,[9] and modulation of both the kinetics and the thermodynamics of DNA binding.[10,11]

Many metallointercalators include dipyridophenazine (dppz) in their coordination sphere, but very few show simultaneous covalent and intercalation binding modes without the need to irradiate them (adducts formation based on photoexcited states). Examples of mononuclear complexes with an exchangeable monodentate ligand include $[Ru(H_2O)(dppz)(tpy)]^{2+}$ [12] and $[IrCl(\eta^5\text{-}Cp^*)(dppz)](CF_3SO_3)$,[11] while $[\{Ir(\eta^5\text{-}Cp^*)(dppz)\}(\mu\text{-peptide-}\kappa S{:}\kappa N)\{trans\text{-}(PtL_2L')\}]^{4+}$ (L, L′ = H_2O, NH_3, dmf)[6] constitute examples of heterobinuclear complexes with linked components that show different DNA binding modes.

The two developed methodologies for dual-binding mode, above indicated, have their own drawbacks. For instance, *cis*-$[CoCl_2(dppz)_2]^+$ shows a relatively rigid octahedral geometry that does not give it enough flexibility for combined binding.[13] Another example is $[IrCl(\eta^5\text{-}Cp^*)(dppz)](CF_3SO_3)$, which prefers covalent binding, since neither a viscosity increase or a significant increase in the DNA denaturation temperature is observed after incubation with the complex.[11] In the second method, the possibility of combined interaction modes depends on the size and flexibility of the bridging ligand.[6]

In this work, we present a different strategy to obtain compounds with an intercalation−coordination dual-binding mode. It consists of the use of metal cations that are flexible enough, concerning either geometry or coordination number, being able to lose or accommodate extra ligands.[14] Partial release of binding ligands is expected to make space for nucleobase during interaction of the complexes with DNA.

We chose the biologically relevant metal centers of copper and zinc with the intercalator dppz and prepared complexes $[Cu(CH_3COO)(dppz)_2]CH_3COO$, **1**, $[Zn(dppz)_2](BF_4)_2$, **2**, and $[Cu(dppz)_2]NO_3$, **3**. After full characterization, we explored their DNA binding mode by thermal denaturation, circular dichroism, viscosimetry, and ESI-MS techniques. Complementary studies by atomic force microscopy (AFM) between circular plasmid pBR322 DNA and **1** were also conducted.

We also decided to test the leishmanicidal activity of **1** and **2**, since the tetrafluoroborate analogue of **3** had been previously evaluated in *Leishmania mexicana* promastigotes, and it was suggested that its activity was related with its ability to intercalate into DNA nucleobases and not to an eventual covalent binding.[15] The same authors also prepared two Cu(II)−dppz complexes,[14k] $[Cu(NO_3)(dppz)]NO_3$ and $[Cu(NO_3)(dppz)_2]NO_3$, which are active against *Leishmania braziliensis* promastigotes.

Leishmaniases are parasitic diseases caused by protozoan flagellates of the genus *Leishmania*, endemic in 98 countries, and presents three clinical forms: visceral (VL), mucocutaneous (MCL), and cutaneous (CL). The first one is the most severe form and potentially leads to death if untreated. The WHO has estimated 1.5 million new cases of CL and 0.5 million of VL per year.[16] Interestingly, it is known that copper and zinc metal ions have serum levels significantly altered both in canine or in human leishmaniasis cases (lower levels of zinc and higher in copper than those of healthy controls).[17,18] Zinc deficiency in VL and MCL indicates a possible therapeutic administration on these severe forms,[18] while oral zinc sulfate is known to be a safe therapy for the cutaneous variation.[19]

Available treatment options on the market include pentavalent antimonials (sodium stibogluconate or meglumine antimoniate), the polyene amphotericin B (as deoxycholate salt or a liposomal formulation), the alkylphosphocholine miltefosine, and the aminoglycoside paromomycin.[20] However, all current treatments suffer from significant drawbacks (i.e., parenteral route of administration of first line drugs, length of treatment, toxicity, and cost, which limits their utilization in endemic areas).[21] Thus, screening for novel compounds against this disease is needed particularly to overcome the main disadvantages of the existing ones and avoid the emergence of drug-resistant strains.

2. EXPERIMENTAL SECTION

2.1. General Data and Physical Measurements. Elemental analyses (C, H, N) were performed by Intertek−QTI (Whitehouse, NJ). Infrared spectra were acquired by diffuse reflection infrared Fourier transform (DRIFT) on a Thermo Nicolet 6700 spectrometer. Samples were run as KBr mixtures (2% w/w compound) (128 scans on 4000−400 cm^{-1} range with 2 cm^{-1} resolution). ^1H NMR spectra of **2** were acquired on a 400 MHz Varian Unity spectrometer, with chemical shifts referred to dmf-d_7 residual protons. UV−vis spectra were obtained on a Jasco V-560 spectrophotometer at 20 °C. QTof-ESI-MS of compound **1** was acquired on negative mode in a methanol solution at a cone voltage of 30 V. It required slow injection (5 μL/min) and some minutes reducing at the needle prior to detection. The QTof-ESI-MS spectrum of complex **2** was acquired in positive mode at 30 V after solubilization in methanol + 1% TFA.

2.2. Molecular Modeling. All calculations were performed on the bach.vcu.edu cluster at the Center for High Performance Computing (VCU) using the Gaussian 03 program, version D2.[22] The "Bach" cluster consists of a total of 764 AMD Opteron 64-bit cores, each with a minimum of 2 GB/core RAM, 14 TB internal disk storage, 1 TB total RAM, 2 TB of/home space, and/tmp space of 50−164 GB per node. Networking infrastructure is gigabit Ethernet. DFT calculations were performed with the hybrid functional B3LYP, which includes HF exchange, Slater's exchange, VWN local correlation, Becke's 1988 exchange,[23] and Lee−Yang−Parr correlation (LYP),[24] with optimization requesting fine grid accuracy for energy and gradient. The high-quality 6-311+G(2d,p) basis set was used for all atoms using three intermediate quality basis sets for "building the guess", 3-21G*, 6-31G(d), and 6-311G(d,p) − while input structures correspond to MM2-minimized structures prepared with the Chem3D Ultra v.8.0 program. A potential energy variation curve was built for $0° \leq \varphi \leq 180°$ in 10° increments, assuming the most stable structure as energy reference. Each pseudoconformer was obtained with the maximum possible symmetry (D_{2h} for 0°, D_2 for 10−80°, and D_{2d} for 90°) since the energy and structure is only marginally affected compared with symmetry free optimizations. The mole fractions, X_i, for the conformers were determined from ΔE_i, using the Boltzmann distribution law, that is, $X_i = \exp(-\Delta E_i/RT)/[\Sigma_j \exp(-\Delta E_j/RT)]$. The standard deviation of the dihedral angle (σ_φ) and its confidence interval were determined with a Gaussian fit. Minimized structures with no restrictions correspond to local minima in the potential energy surface, since no negative values were found on their vibrational determined frequencies. ChemCraft[25] was used as the visualization and illustration program.[26] Energy-minimized structure coordinates and selected bond distances and angles are presented in the Supporting Information.

2.3. Biophysical Studies. Highly polymerized cT-DNA Type I from Sigma was solubilized in DD-H_2O by gentle inversion overnight at 0−4 °C, desalted (48 h at 4 °C) using a 12−14 kDa cutoff dialysis membrane, lyophilized, solubilized in 10 mM Tris +10 mM $NaClO_4$, adjusted to pH 7.4 with perchloric acid, and kept at 4 °C for up to 48 h. For longer periods, it is kept frozen and protected from light. CT-DNA solutions titles were determined by UV−vis at room

dx.doi.org/10.1021/ic401067d | Inorg. Chem. 2013, 52, 8881−8894

temperature, measuring the absorbance at 260 nm, in triplicate, and considering ε_{DNA} = 6600 M^{-1} cm^{-1} per nucleotide.[27] Purity of the solution was confirmed by the ratio of measured absorbances at 260 and 280 nm.[28] Due to lack of solubility of some of the compounds in aqueous environments, particularly **3**, the ct-DNA solutions used on the interaction studies correspond to a 20:80 v/v organic/aqueous mixture, where the organic solvent fraction is DMSO (**1** or **2**) or DMF (**3**). DMF was used in all experiments with **3** since it easily oxidizes in DMSO. The organic fraction was limited to 20% v/v to avoid changes on DNA conformation and drug accessibility to their targets (confirmed by circular dichroism). A title of 750 μM in the organic solvents permits one to prepare such mixtures if careful aliquot addition is conducted. No chloride was present on the buffer to avoid formation of chloro pentacoordinated complexes and mimic low chloride concentration inside the cells. Vials with the oligonucleotides *ds*(GCGCGCGC) and *ds*(GCGCGCGCGC) (from Thermo Fischer Scientific GmbH), from now on named 4GC and 5GC, are warmed at 85 °C for 45 min on a heating block, kept overnight at room temperature, protected from light, and then maintained at 4 °C until use (less than 48 h). Oligonucleotide solutions were prepared in 0.5 M ammonium acetate.

2.3.1. Thermal Denaturation. A 200 μM ct-DNA was used in all experiments, with incremented complex concentration from 0 to 25 μM. Samples were degassed for 5 min with a ThermoVac Sample Degasser (MicroCal, General Electric Healthcare) prior to use. Thermal denaturation studies were followed measuring continuously the absorbance (A) at 260 nm on a Jasco V-560 spectrometer with a 30 W deuterium lamp. Samples were placed on a far UV quartz sub-micro low headspace cell cuvette from Starna and sealed with a PTFE stopper. It was heated with a circulation water jacket at a heating rate of 0.5 °C/min that correlates linearly with the temperature in the cell, measured with a Peltier element. Temperature and time correlate linearly according the following equation: T (°C) = 0.0084t (s) + 37.801 (R^2 = 0.998). The increase in the absorbance was normalized with the formula $(A - A_o)/(A_{max} - A_o)$ and fitted with a sigmoidal curve to determine the melting temperature, T_m, that is the temperature that results on average in an 1:1 equilibrium between denaturated and nondenaturated ct-DNA.

2.3.2. Circular Dichroism. Formulations with complexes **1**–**3** and ct-DNA were incubated at room temperature for 1 h. The amount of drugs was incremented while keeping the ct-DNA concentration constant at 100 μM. Circular dichroism (CD) spectra were acquired at room temperature in a nitrogen atmosphere with a Jasco J-600 spectropolarimeter. The device was calibrated with D-camphorsulfonic acid. A quartz sub-micro cuvette with a 1 cm path length was used on all experiments. Spectra were acquired on the 235–450 nm range. Each sample was scanned three times, and the spectra were averaged. Electronic subtraction of the background was then performed. Two independent samples were measured at each drug concentration.

2.3.3. Rheometry. Complexes were solubilized in DMSO (**1**, **2**, and ethidium bromide) or DMF (**3**) at 750 μM and diluted with aliquots of 10 mM Tris-buffer/10 mM $NaClO_4$ at pH 7.4 and by ct-DNA in the same buffer to achieve a final volumetric ratio of organic solvent/aqueous buffer of 20:80. A constant concentration of 600 μM ct-DNA was used with [M]/[DNA] ratios between 0 and 0.25. Mixtures were left at room temperature to incubate for 1 h prior to any measure. Each ratio was analyzed by three independent samples. Viscosity, η (mPa/s), was measured at 25 °C on a Thermal Analysis TA AR1500EX rheometer with a cone/plate rotating measuring system (40 mm). Typical conditions consist of a 715–720 μL sample, a 500 μm gap, shear stress limits of 2.5–9 Pa, and shear rate of 0.2–2 s^{-1}, with nine points per decade. Sonication is seldom performed to minimize complexities arising from DNA flexibility, which interfere with the linear improvement of viscosity according to DNA's lengthening. Such procedure is not required for Sigma's highly polymerized type I ct-DNA (according to Sigma, it is obtained with an extraction method that causes shearing and no further sonication is recommended) as confirmed for the classic intercalator ethidium bromide, EtBr, with η/η_o progressing in a linear way up to DNA saturation (R = 0.25). Compared to capillary viscometers, more commonly used on DNA intercalator studies, rheometers are less sensitive (typical error on the selected equipment is 3–4 × 10^{-5} Pa·s) and require higher concentrations to increase viscosity to an order of magnitude of 10^{-3} Pa·s. Nevertheless, experiments are much faster and associated error depends much less on the human operator. In a preliminary study with EtBr and 375 μM ct-DNA the drug/DNA ratio (R) can go up to 0.40. Results confirm that DNA saturation occurs at R = 0.25 of EtBr, but the associated error is still high. All further studies were then performed with 600 μM ct-DNA that permit achieving R = 0.25 while significantly decreasing the error associated to viscosity determination.

2.3.4. Atomic Force Microscopy. A 200 μM stock solution of complex **1** in DMSO was successively diluted with HEPES buffer (40 mM at pH 7.26) up to a 0.0552 nM title, while a circular plasmid pBR322 DNA (Sigma) stock solution with a title of 2.76 nM (nucleotides) was prepared in the same HEPES buffer. The mica disk was treated for 15 min with a APTES (3-aminopropyltrietoxysilane)/HEPES buffer (40 mM at pH 7.26), 1:5 v/v mixture in order to modify its surface and make it able to immobilize the DNA molecules, washed with 1 mL of DD-H_2O, and dried under a flow of nitrogen. Interaction studies of **1** with plasmid DNA were conducted in air at room temperature after 1 h incubation at room temperature for **1**:DNA molar ratios of R = 0, 0.125, 0.250, and 0.500, keeping a fixed DNA concentration (27.6 pM). For each preparation, 10 μL was placed on the mica disk and let interact for 15 min. A 1 mL amount of DD-H_2O and doubly filtered on a Millipore membrane was used to wash the mica that was thoroughly dried under nitrogen. Scanning was conducted on a Digital Instruments/Veeco Inc. equipment. Under the experimental conditions, a high number of well-separated single DNA molecules were observed (15–25 molecules on an initial window of 5 × 5 nm). The Nanoscope v530.3SR3 program was used for data treatment, while the program ImageJ 1.44p (NIH) was used to determine the length of the plasmid DNA. Measurements were performed at 1024 × 768 pixels resolution on 2 × 2 nm windows (for 12 single molecules with length determined in triplicate and error margin determined at the 2σ level).

2.3.5. QTof-ESI-MS. Oligonucleotides were solubilized in 0.5 M ammonium acetate, while compounds were solubilized in methanol. The two solutions were mixed at a methanol/ammonium acetate buffer ratio of 3:1 v/v, incubated for no less than 1 h, and centrifuged at 14k rpm for 10 min, and the supernatant was injected at 10 μL/min. For each complex (M) and oligonucleotide (4GC or 5GC) both 1:1 and 3:1 M/oligonucleotide proportions were tested. Prepared concentrations were 33.3 and 100 μM for the complexes and 100 μM for 4GC or 5GC. Since on ESI-MS the concentrations are measured per oligo (ss) molecule and not per nucleotide, as in the other described biophysical studies, converting these ratios to the same system results in R values of 0.125 and 0.375 for 4GC and 0.100 and 0.300 for 5GC, respectively. A cone voltage of 20–25 V was determined to give the best-combined conditions to maximize the relevant peaks intensity and minimize fragmentation of the oligonucleotides double strand. Other conditions were used whenever justified, particularly for tandem experiments on ions of small abundance or easy fragmentation. Other experimental conditions related with the equipment were according to the literature.[29] MS/MS were determined with the same device and experimental conditions previously used by some of us to study recognized intercalators,[30] since it is known that both variables have an impact on the fragmentation of noncovalent ions. A supplementary difficulty for assignment of the species interacting with the oligonucleotides resides on the small m/z differences of multiple charge ions that normally occur. Since oligonucleotide calibration employs a multipeak fitting that minimizes the global error, it implies that some regions might have a significant deviation. A second adjustment was then performed for different regions of the spectrum, based on the deviation found on the peak of higher intensity of each interval: for $[ss]^{3-}$ when below its m/z value, for $[ds]^{4-}$ when m/z is between $[ss]^{3-}$ and $[ds]^{4-}$, and for $[ds]^{3-}$ when m/z is above $[ds]^{4-}$.

2.4. Drug Cytotoxicity. Macrophages derived from human caucasian histiocytic lymphoma U-937 cell line (ECACC 85011440,

dx.doi.org/10.1021/ic401067d | Inorg. Chem. 2013, 52, 8881–8894

U.K.) in the logarithmic phase of growth were incubated in 96-well plates in 0.2 mL complete RPMI-medium containing 50 ng/mL of phorbol 12-myristate 13-acetate (PMA, Sigma) for 48 h to induce differentiation.[31] Differentiated U-937 cells were washed three times with fresh medium containing no PMA prior to addition of the compounds. Due to the reduced solubility of some drugs, the complexes were solubilized in DMSO at 750 μM and then diluted with RPMI to 30 μM (4% DMSO v/v). Miltefosine was directly solubilized in RPMI medium at 250 μM. Maximum tolerated dose (MTD_{25}) of U-937, i.e., the drug concentration causing a 25% decrease in viable cell number, was determined by serial dilutions of the compounds in complete RPMI medium. This condition (less than 4% v/v DMSO) is noncytotoxic to the promastigote cultures or line cell. DMF was excluded because of its much higher cytotoxicity. To avoid significant oxidation of compound **3** in DMSO, solubilization was performed in no more than 10 min and immediately frozen under liquid nitrogen, until ready to use. After 2 h of incubation with sodium-2,3-bis[2-methoxy-4-nitro-5-sulfophenyl]-2*H*-tetrazolium-5-carboxanilide (XTT assay from Roche Diagnostics), cell viability was determined by electronic spectroscopy, with three independent experiments performed in triplicate, measuring the amount of reduced XTT (OD values were determined at 450 nm with a 650 nm reference filter),[32] with MTD_{25} determined by linear and nonlinear regression analysis of the log levels of concentration (μM) on cell viability (%). Results for linear analysis were expressed as the media ± standard deviation, while the modeling of the nonlinear effect was performed with the software R[33] using a Generalized Additive Model (GAM) based on P-Splines estimation with smoothness selection by REML (Restricted Maximum Likelihood).

2.5. Parasite Drug Susceptibility. The *Leishmania infantum* MHOM/PT/88/IMT-151 strain, isolated from a human visceral leishmaniasis case, was used in this study. The promastigote forms of the parasite were cultured at 24 °C in complete RPMI medium (RPMI medium (Sigma), at pH 7.2, supplemented with penicillin (10 000 U/mL), streptomycin (10 mg/mL), and 10% heat-inactivated fetal calf serum from FCS-Gibco, USA).[31] In vitro susceptibility tests for the formulations of **1**−**3** and miltefosine (AEterna Zentaris, Inc.), used as the reference drug, were performed on 1×10^6 *L. infantum* promastigotes/mL in the stationary phase of in vitro growth. The promastigote culture aliquots (in RPMI) were added to a dilution series of the compounds. Tests were performed in 96-well microtiter plates after 2 days of incubation at 24 °C. The parasitic viability parameter was determined with the XTT kit as previously described (see section 2.4). The intramacrophagic amastigote in vitro sensitivity to the compounds was also assessed. To this purpose, the cell line U-937, kept in complete RPMI medium containing 50 ng/mL of phorbol 12-myristate 13-acetate (PMA, Sigma), was differentiated and infected with promastigotes at the stationary growth phase. After 24 h of drug incubation, the number of infected cells was determined by optical microscopy (number of macrophages infected with respect to 100 cells), the same as the infection intensity (number of parasites per macrophage).

2.6. Syntheses. All solvents used were of pro analysis or superior quality. All chemicals were acquired from established international suppliers and used without further purification. Dipyridophenazine (dppz) and $[Cu(dppz)_2]NO_3$, **3**, were prepared according to the literature.[34,35] Complex **2** was synthesized under nitrogen atmosphere using Schlenk techniques, while complex **1** was prepared under air.

*2.6.1. $[Cu(CH_3COO)(dppz)_2]CH_3COO$ (**1**).* A 291 mg amount of dipyridophenazine hemihydrate (1 mmol) and 100 mg of copper(II) acetate monohydrate (0.5 mmol) were mixed in methanol and heated under reflux for 2 h, and a deep green solution formed. It was evaporated to dryness and washed with ether under ultrasounds. After filtration, it was dried under vacuum overnight (yield 342 mg; 74%). Anal. Calcd for $C_{40}H_{26}CuN_8O_4 \cdot 3\ H_2O$: C, 60.03; H, 4.03; N, 14.00. Found: C, 59.85; H, 4.04; N, 14.04. FT-IR (KBr, cm^{-1}): 3080, 3056, 2926, 1594 + 1581, 1495, 1465, 1420, 1390 + 1380, 1358, 1341, 1234, 1212, 1187, 1137, 1094, 1075, 1048, 1011, 924, 903, 821, 768, 733, 719, 675, 641, 618, 426. UV−vis (DMF) λ_{max}, nm ($\varepsilon \times 10^{-3}$ M^{-1} cm^{-1}): 600−700 (60), 380 (28.1), 369 sh, 361 (26.9), 351 sh, 343 sh, 270 (116.3). QTof-ESI-MS(−) (in MeOH; *m*/*z*; RI*,§): 282.1 ($dppz^-$; 66%*, 60%§), 404.2 ($\{Cu(CH_3COO)(dppz)\}^-$; 7%*,§), 627.0 ($[Cu(dppz)_2]^-$; 79%*, 9%§) ((*) concentrated solution; (§) diluted solution). MS/MS (35 V) of 627.11 (−): 344.0 ($\{Cu(dppz) - H\}^-$) and 282.1 ($dppz^-$). MS/MS (35 V) of 404.22 (−): 282.1 ($dppz^-$).

*2.6.2. $[Zn(dppz)_2](BF_4)_2$ (**2**).* A 174 mg amount of $ZnBF_4 \cdot 6\ H_2O$ (0.5 mmol) and 291 mg of dipyridophenazine hemihydrate (1 mmol) were mixed in 30 mL of degassed absolute ethanol. The suspension was heated at 60 °C for 2 h and filtered while hot. Collected white solid was washed with diethyl ether and dried overnight at 60 °C (yield 124 mg; 31%). Anal. Calcd for $C_{36}H_{20}B_2F_8N_8Zn \cdot 0.5\ H_2O$: C, 53.21; H, 2.60; N, 13.79. Found: C, 53.26; H, 2.63; N, 13.75. . ^{1}H NMR δH (dmf-d_7), ppm: 9.96 br ($H^{3/6}$), 9.17 br ($H^{1/8}$), 8.54 br ($H^{10/13}$), 8.34 br ($H^{2/7}$), 8.25 *dd* ($H^{11,12}$, J_{1-2} = 8.4 Hz; J_{1-3} = 4.4 Hz). FT-IR (KBr, cm^{-1}): 3110, 3089 + 3068 + 3049 + 3040, 1626, 1607, 1592, 1583, 1550, 1498, 1470, 1448, 1423, 1362, 1339, 1323, 1284, 1265, 1237 + 1231, 1193, ca. 1060 (br, vs) from BF_4^- overlaps other bands at 1142, 1125, 1096, 1078, 1053, 1015, 990 and 960, 902, 845, 825, 763, 736, 716, 650, 638, 618, 579 + 573, 521, 426. UV−vis (DMF) λ_{max}, nm ($\varepsilon \times 10^{-3}$ M^{-1} cm^{-1}): 379 (23.9), 369 sh, 360 (23.2), 350 sh, 342 sh, 272 (95.6). QTof-ESI-MS(+) (in MeOH + 1% TFA; *m*/*z*; RI): 283.1 ($\{dppz + H\}^+$; 100%), 313.6 ($\{[Zn(dppz)_2] - H\}^{2+}$; 2%), 459.1 ($\{Zn(dppz) + TFA\}^+$; 58%), 627.2 ($\{[Zn(dppz)_2] - H\}^+$; 1%), 740.2 ($\{[Zn(dppz)_2 + TFA - H\}^+$; 62%).

3. RESULTS AND DISCUSSION

3.1. Chemical Discussion. Cu(II)−dppz complexes with chloro, aquo, and nitrato ligands have been previously prepared

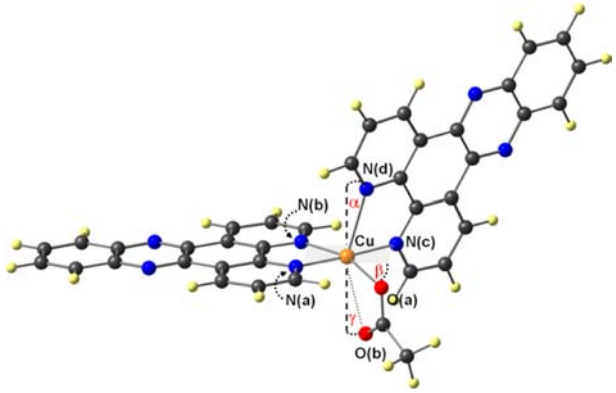

Figure 1. Optimized structure of $[Cu(k^1\text{-}CH_3COO)(dppz)_2]^+$, **1** (B3LYP/6-311+G(2d,p)), and representation of the relevant distortions angles α, β, and γ.

with $[Cu(H_2O)(dppz)_2](ClO_4)_2$ and $[CuCl(dppz)_2]Cl$ showing distorted trigonal bipyramidal and distorted square pyramidal geometries, respectively.[14j,36] For $[Cu(NO_3)(dppz)_2]NO_3$, a distorted octahedral geometry (nitrate in a bidentate coordination mode) was proposed based on EPR results and HF/3-21G* calculations.[14k]

Complex **1** was prepared under air from copper acetate and dppz in refluxing methanol and isolated as a light green compound. Elemental analysis and infrared confirm the presence of acetate in the solid. Elemental analysis agrees on a 1:2:2 Cu−dppz−acetate ratio, while infrared shows a broad band with maxima at 1610−1575 cm^{-1}, where $\nu_{as(COO-)}$ is expected, and a second and sharper one at 1385 cm^{-1}, typical of $\nu_{s(COO-)}$ (Figure S1, Supporting Information). Two maxima are observed on the high-energy component. The one at lower frequency comes probably from ionic acetate, while the higher frequency gives a difference of 215 cm^{-1} between the

dx.doi.org/10.1021/ic401067d | Inorg. Chem. 2013, 52, 8881−8894

Table 1. Coordination Sphere Comparison between Calculated and X-ray Structures of $[Cu(CH_3COO)(dppz)_2]^+$, 1^+, and $[Cu(RCOO)(phen)_2]^+$ (R = H, CH_3, $C_6H_5CH_2$)

	$[Cu(CH_3COO)(dppz)_2]^+$, DFT	$[Cu(CH_3COO)(phen)_2]^+$, X-ray (ref 42)	$[Cu(C_6H_5CH_2COO)(phen)_2]^+$, X-ray (ref 41b)	$[Cu(CH_3COO)(phen)_2]^+$, X-ray (ref 41a)	$[Cu(HCOO)(phen)_2]^+$, X-ray (ref 41c)
Cu−N(a)	2.0528 Å	2.0152 Å	2.0131 Å	1.9878 Å	1.9771 Å
Cu−N(b)	2.1021 Å	2.0366 Å	2.0599 Å	2.0507 Å	2.0593 Å
Cu−N(c)	2.0717 Å	2.0219 Å	2.0008 Å	1.9893 Å	1.9853 Å
Cu−O(a)	1.9646 Å	1.9522 Å	2.0013 Å	2.0013 Å	2.0197 Å
Cu−N(d)	2.3451 Å	2.2449 Å	2.1863 Å	2.1930 Å	2.1767 Å
Cu−O(b)	2.5872 Å	2.7649 Å	2.7153 Å	2.6401 Å	2.7665 Å
N(d)−N(d′)	0.59 Å	0.79 Å	0.53 Å	0.67 Å	1.01 Å
α	14.7°	20.7°	14.1°	17.8°	27.5°
O(a)−O(a′)	0.55 Å	0.15 Å	0.63 Å	0.93 Å	1.10 Å
β	16.3°	4.4°	18.3°	27.8°	32.9°
O(b)−O(b′)	0.80 Å	1.51 Å	0.90 Å	0.38 Å	0.34
γ	18.0°	33.1°	19.4°	8.3°	7.0°
τ	0.23	0.04	0.23	0.42	0.51

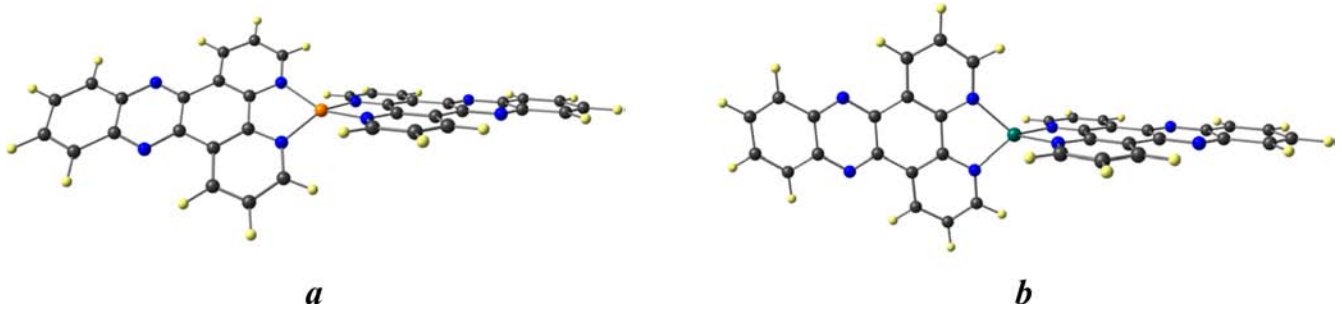

Figure 2. DFT-optimized structures of $[Cu(dppz)_2]^{2+}$ (a) and $[Zn(dppz)_2]^{2+}$ (b) at the B3LYP/6-311+G(2d,p) level.

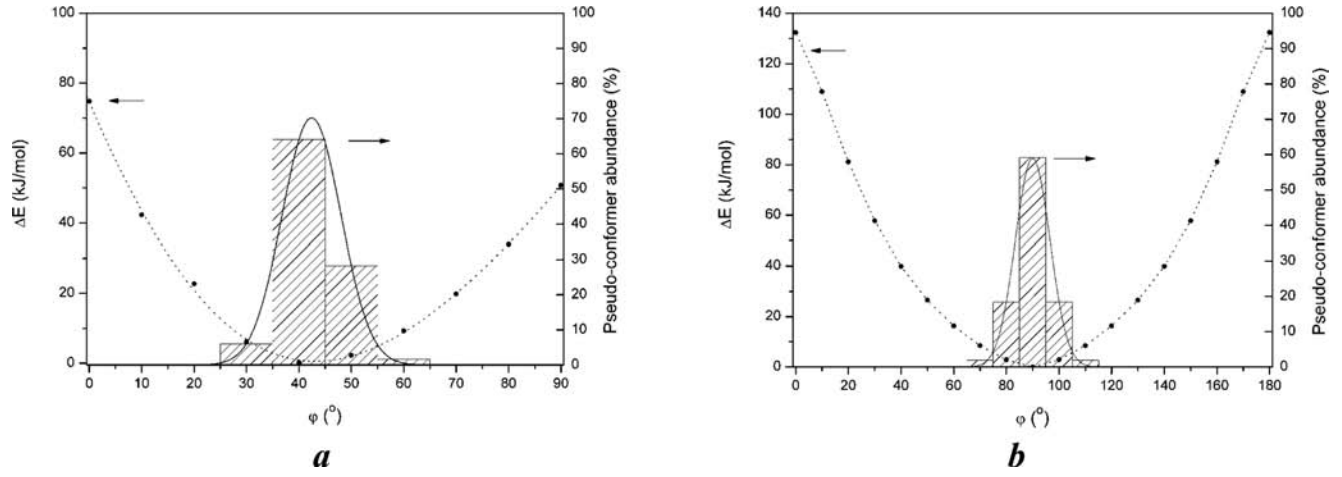

Figure 3. Energy profile (---) of pseudoconformers (●) with $0° \le \varphi \le 90°$ for $[Cu(dppz)_2]^{2+}$ (a) and $0° \le \varphi \le 180°$ for $[Zn(dppz)2]^{2+}$ (b); pseudoconformer abundance according a Boltzmann distribution and their Gaussian fitting (—). All calculations at the B3LYP/6-311+G(2d,p) level.

asymmetric and the symmetric modes of the carboxylate, which indicates a k^1 binding mode of acetate,[37,38] that is, $[Cu^{II}(k^1\text{-}CH_3COO)(dppz)_2](CH_3COO)$.

All known Cu(II)−RCOO−dppz coordination compounds, 2D chains, or 3D clusters, where the carboxylates bind to a single copper center, have a k^1-COO coordination mode,[39,40] indicating a strong preference for such binding. Structurally equivalent Cu(II)−RCOO−phen complexes show the same binding mode preference and a common distorted square pyramidal geometry.[41,42]

QTof-ES-MS(−) of **1** in methanol under mild to moderate energies (cone voltage at 20−35 V) show a clear preference for the form $[Cu(dppz)_2]^-$, suggesting the weak binding of acetate. The only ion that can possibly indicate bound acetate is the low abundant one at m/z 404.2, assigned to $\{Cu(CH_3COO)(dppz)\}^-$. Loss of dppz ligands is also marginal at best as shown by the low abundance of the ion at m/z 345.0 ($[Cu(dppz)]^-$). In aqueous solutions, acetate exchange with water should be fast and complete. Under an excess of acetate, as in ESI-MS biophysical studies, the compound is considered to be present

dx.doi.org/10.1021/ic401067d | Inorg. Chem. 2013, 52, 8881−8894

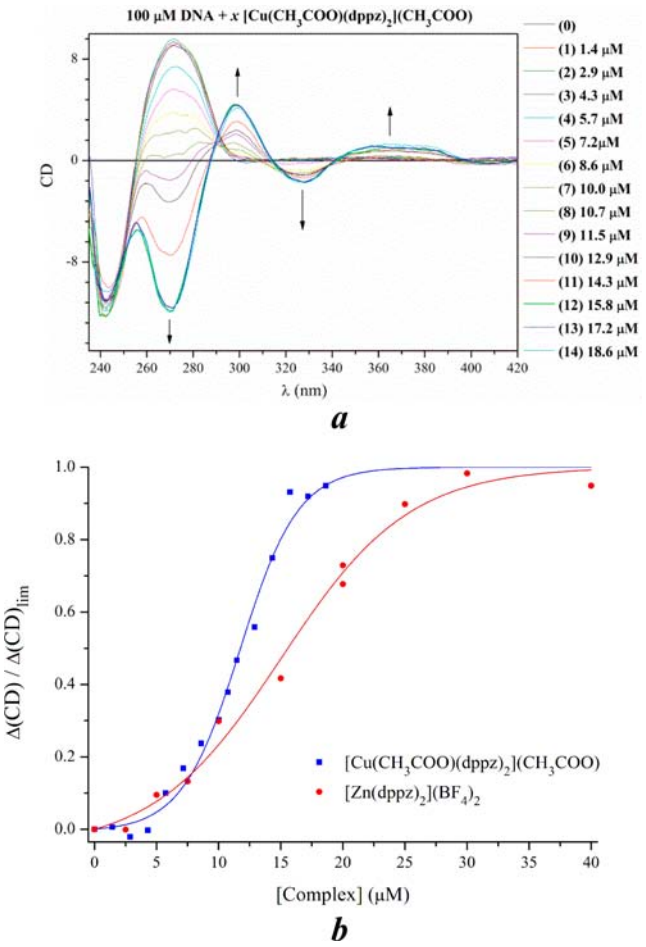

Figure 4. (a) ICD spectra of DNA titration with $[Cu(CH_3COO)(dppz)_2]CH_3COO$, **1** (0−18.6 μM), and (b) normalized intensity variation at 270 nm for complex **1** (0−18.6 μM) and $[Zn(dppz)_2](BF_4)_2$, **2**, (0−40 μM). All measurements with 100 μM ct-DNA in 1:4 DMSO/(10 mM Tris + 10 mM $NaClO_4$).

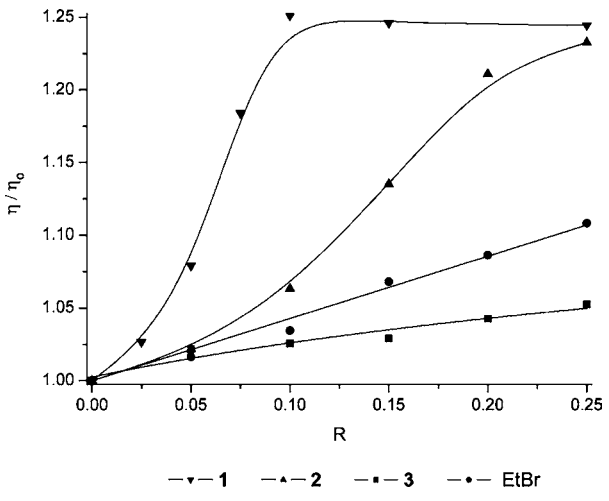

Figure 5. Evolution of the relative viscosity of DNA/drug mixtures at 25 °C with R = [M]/[DNA] (≤0.25). Experimental conditions: 600 μM ct-DNA in 1:4 Solv/10 mM Tris + 10 mM NaClO4, at pH 7.4 (Solv = DMSO for **1** and **2** and EtBr and DMF for **3**).

in the original form (see discussion for **2**, below), but its loss is expected when the compound binds the oligonucleotides and should not be detected as such.

Compound **2** was prepared in nitrogen degassed hot ethanol from $Zn(BF_4)_2{\cdot}6H_2O$[43] and dppz and isolated by filtration while hot. Elemental analysis, ESI-MS, and NMR confirm its purity. ^{1}H NMR (dmf-d_7) of **2** is characterized by broad aromatic environments on $H^{1/8}$, $H^{2/7}$, $H^{3/6}$, and $H^{10/13}$. Only the signal near 8.25 ppm, assigned to the protons further away from the metal ($H^{11/12}$), is resolved at room temperature. Other dppz complexes, like **3**, are known to have broad NMR environments at room temperature, a phenomenon justified by the torsion around the dihedral angle defined by the two dppz ligands on the coordination sphere of the metal cation (φ).[35] Such results indicate that while expectedly tetrahedral, **2** should not have a rigid D_{2d} symmetry at room temperature.

QTof-ES-MS(+) of **2** in methanol acidified with 1% v/v of TFA reveal that the large excess of TFA is able to associate the metal. In fact, the zinc ions associated with TFA ($[Zn(TFA)(dppz)]^+$ and $\{[Zn(TFA)(dppz)_2] - H\}^+$) are largely more abundant than the ones without it. This confirms the flexibility of zinc ion to accommodate other ligands in its coordination sphere.

3.2. Molecular Modeling. Combined information, above mentioned, indicates that the formula of **1** in the solid state is most probably $Cu(k^1\text{-}CH_3COO)(dppz)_2](CH_3COO)$. Our results, at the B3LYP/6-311+G(2d,p) level of theory, support the proposed formula (see Figure 1).

Flexible pentacoordinated structures can easily distort between trigonal bipyramidal and square pyramidal geometries and interconvert between them by a mechanism known as Berry pseudorotation. The more common way to evaluate such distortions is the tau parameter (τ) determined by the angular difference between the two larger angles divided by 60°. Perfect square pyramidal and trigonal bipyramidal geometries give τ of 0 and 1, respectively. Intermediate values of τ indicate the degree of deviation from perfect geometries. X-ray crystal data for a few $[Cu(RCOO)(phen)_2]^+$ (R = H, CH_3, $C_6H_5CH_2$) complexes are presented in Table 1, where τ varies between 0.04 and 0.51. The DFT-minimized structure of $\mathbf{1}^+$ gives τ = 0.23, well in the middle of the interval of τ, indicating that it is a slightly distorted square pyramidal structure.[44] The positions at the base are occupied by two nitrogen atoms of one dppz, N(a) and N(b), one nitrogen atom from the second dppz, N(c), and one oxygen atom of acetate, O(a). A second nitrogen atom of the second dppz, N(d), binds near the apex. The DFT structure shows several atoms coordinated with an angular orientation that deviates from the square pyramidal geometry. While N(a), N(b), N(c), and Cu atoms sit in the pyramid base, O(a) is below such plane by 0.55 Å (β = 16°). Furthermore, the Cu−N(d) bond deviates from the zz' axis by 15° (α) or 0.59 Å to the apex. O(b), which only shows a weak interaction to the metal center, is also deviated from zz' by 18° (γ).

Since the τ value has a strong implication on bond lengths and angles and affects evaluation of the level of agreement between DFT and X-ray crystal structures, we only selected $[Cu(C_6H_5CH_2COO)(phen)_2]^+$ for comparisons with $\mathbf{1}^+$ (also has a τ of 0.23). The distortions found in the crystal structure of $[Cu(PhCH_2COO)(phen)_2]^+$, measured by α, β, and γ, are almost identical to the ones observed in $\mathbf{1}^+$, confirming the adequacy of the chosen theoretical method to predict the geometry of the complexes.

The coordination sphere bond lengths of $\mathbf{1}^+$, determined theoretically, show differences between −0.13 and +0.16 Å to the experimental one. Nevertheless, the bigger differences occur in the weak interactions in the zz' axis, which minimize its

dx.doi.org/10.1021/ic401067d | Inorg. Chem. 2013, 52, 8881−8894

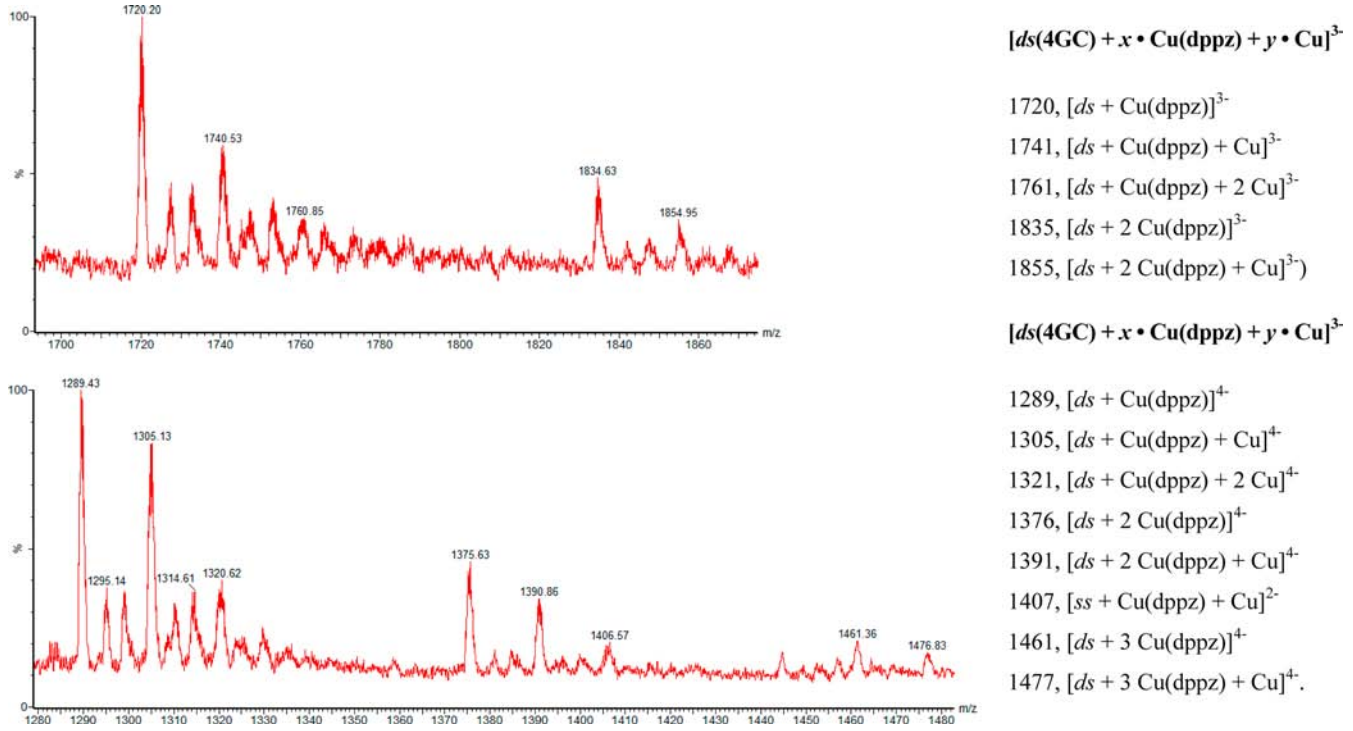

Figure 6. Interaction of *ds*(GCGCGCGC) = *ds*(4GC) with $[Cu(CH_3COO)(dppz)_2]CH_3COO$, **1**: MS spectra regions where the diagnostic ions ($[ds(4GC) + xCu(dppz) + yCu]^{3-/4-}$) occur and respective assignments.

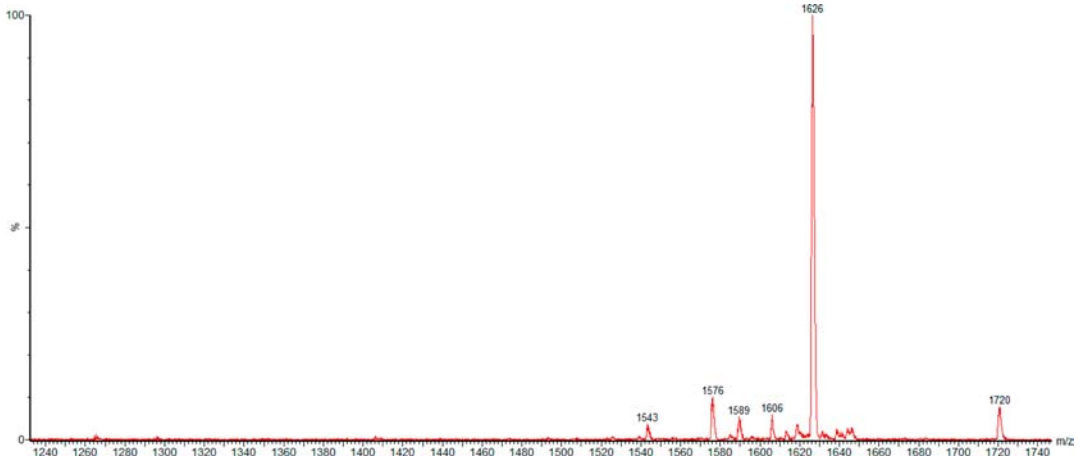

Figure 7. MS^2 spectrum of m/z 1720 ion ($[ds(4GC) + Cu(dppz)]^{3-}$) obtained with a collision energy of 25 eV: 1626, $[ds + Cu]^{3-}$; 1606, $[ds]^{3-}$.

relevancy. If we disconsider them, the differences fall to between −0.04 and +0.07 Å. Such differences are normal when density functionals without dispersion correction, as B3LYP, are used.[45]

QTof-ESI-MS data indicate that in the media used to test the interaction of complexes **1** and **2** with GC oligonucleotides (methanol/ammonium acetate buffer at 3:1 v/v) both compounds are expected to have an associated acetate, while in methanol the major abundant ions should not include associated acetate. Other biophysical tests were conducted in 10 mM Tris + 10 mM $NaClO_4$ buffer/DMSO at 4:1 v/v, favoring $[Cu(dppz)_2]^{2+}$ and $[Zn(dppz)_2]^{2+}$, even if small amounts with associated perchlorate or DMSO might be present. During the interaction with DNA, the extra ligand is expected to be labile. In fact, phosphates on the external surface should compete with them during the external binding preliminary step. Likewise, van der Waals forces and hydrogen bonds, which might be relevant when the compound is on the grooves, and steric clashes present during the compounds migration to their intercalation sites should affect the lability of such ligand in the same way.

As indicated, compounds **1** and **2** were selected to probe the possibility of the intercalation−coordination dual-binding mode mechanism during DNA interactions based on their geometry and coordination number flexibility. To measure the torsion ability of the two compounds (Figure 2), a potential energy curve of $[M(dppz)_2]^{2+}$ (M = Cu^{2+}, Zn^{2+}) for the dihedral angle defined by the two chelate rings (φ) was determined (see Figure 3). The angle was varied between 0° and 90° for **1** and up to 180° for **2** in 10° increments, assuming maximum possible symmetry for each pseudoconformer (D_{2h} for 0°, D_{2d} for 90°, and D_2 for the remaining points). $[Zn(dppz)_2]^{2+}$ has a

dx.doi.org/10.1021/ic401067d | Inorg. Chem. 2013, 52, 8881−8894

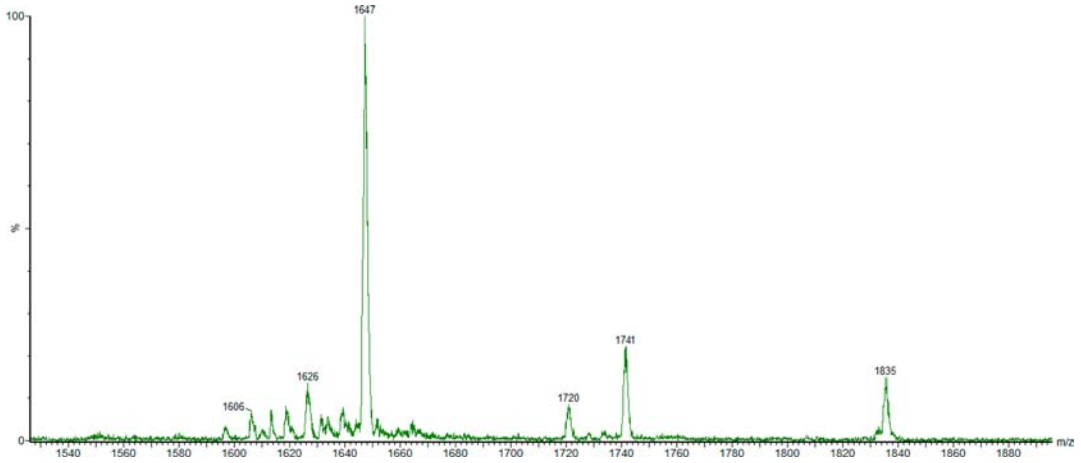

Figure 8. MS^2 spectrum of m/z 1835 ion ($[ds(4GC) + 2\ Cu(dppz)]^{3-}$) obtained with a collision energy of 25 eV: 1741, $[ds + Cu(dppz) + Cu]^{3-}$; 1720, $[ds + Cu(dppz)]^{3-}$; 1647, $[ds + 2Cu]^{3-}$; 1626, $[ds + Cu]^{3-}$; 1606, $[ds]^{3-}$.

minimum at φ = 90° with a symmetrical energy evolution between 0° and 180° and a energy barrier for the parallel pseudoconformer, $E_{||}$, of 132.4 KJ/mol. The pseudoconformer abundance evolution with φ, applying a Boltzmann model to the energy, fits well a Gaussian distribution, with a 95% confidence interval of 90° ± 16.4°. Such variation should be sufficient to justify the broad signals of the ^{1}H NMR of **2**. Compound $[Cu(dppz)_2]^{2+}$ show a 90° periodicity, with a minimum energy at φ = 42.7° and a 95% confidence interval of 11.5°. The energy barriers for the parallel and perpendicular pseudoconformers are unsymmetrical and significantly smaller, with $E_{||}$ = 74.4 KJ/mol and $E_{\perp}$ = 61.7 kJ/mol. These results indicate that the copper complex approximates planarity much more than the zinc analogue. Therefore, it is expected to be more adequate to an easy penetration of DNA, which can then lead to intercalation.

3.3. Stability Studies. While all three complexes are stable in the solid state, they show a distinct behavior in solution. Compound **2** is also stable in solution, but **1** and **3** can interconvert oxidation states under the right conditions. Compound **1** suffers reduction to Cu(I) if placed in 1:4 DMF/Tris. Spectrum evolution can be followed in Figure S2, Supporting Information, until the solution gets saturated with the less soluble Cu(I) compound and precipitates out. Solutions of **1** also tend to reduce when kept protected from light, even if an oxidizing solvent like DMSO is used. Nevertheless, they easily revert to Cu(II) if placed under light and bubbled with air. Compound **3** oxidizes in DMSO solution if oxygen is present, and the reaction can be easily followed in the visible region of the electronic spectrum due to loss of the solution's intense orange color. Even under nitrogen, oxidation still occurs if the solution is kept under natural light. Light absorption at the UV range is enough to cause oxidation by itself even under reducing conditions (DMF/N_2) as seen in Figure S3, Supporting Information. This process is strongly accelerated with UV laser light (30% oxidation after 1 min irradiation at 254 nm). While temperature accelerates the process, heating is not enough to cause oxidation of **3** if only visible light is used during spectra acquisition. The solution regains its orange/red color, characteristic of Cu(I)−polypyridyl complexes, when ascorbic acid is added, giving further support to the reversible redox process.

3.4. Polynucleotide Interactions. *3.4.1. Thermal Denaturation of DNA.* Lack of redox stability of **1** and **3** under the experimental conditions required to study DNA thermal denaturation (see section 3.3) limited this study to compound **2**. It causes a significant increase of the melting temperature, T_m (Figure S4, Supporting Information), of ct-DNA, as expected for a metallointercalator. At R = 0.125 the value of ΔT_m is 9.4 °C, which is slightly above the observed increment for EtBr (8.8 °C). For the same range, ΔT_m for **2** deviates more from linearity than EtBr.

3.4.2. Induced Circular Dichroism. B-DNA show two characteristic bands near (−) 245 and (+) 270 nm, which are assigned to its helicity and nucleobases π stacking. Intercalators are known to stabilize both these bands, while a simple electrostatic interaction or groove binding results in no to small change.[46]

Compounds **1**−**3** are CD inactive, but addition of **1** or **2** to B-DNA has a significant impact on the polynucleotide spectrum. The helicity band suffers only a slight stabilization during the titration, but there is complete signal inversion of the second one. The two compounds induce the same band profile, with ICD bands at (−) 270, (+) 300, (−) 325, and (+) 350−390 (Figure 4a). Four isodichroic points are observed near 250, 290, 310, and 340 nm, confirming that ICD signals result from equilibria between two species in solution: DNA and the DNA−complex adduct. The negative band near 320 nm is very characteristic of dppz complexes[6,11,47] and has been assigned to the existence of an intercalated form, and both **1** and **2** are expected to behave as metallointercalators. The positive ICD band at 350−390 nm coincide with the wavelength of the very characteristic electronic transitions of dppz and its complexes, known as "double humps" (see Figures S2 and S3, Supporting Information). The signal inversion (+ → −) at 270 nm is not so common among intercalators,[11,47,48] but a few examples with dppz complexes are known. Chen et al. (2008)[48b] have shown that $[Ru(dppz)(Me\text{-}im)_4]^{2+}$ results in a positive band at 275 nm, while $[Ru(dppz)(im)_4]^{2+}$ induces a change in sign at (−) 277 nm. They proposed that hydrogen bonds between the HN^1-imidazole and NH_2/NH or O=/OH groups of nucleobases, which are not possible in MeN^1-imidazole, would help to fix the structure, making possible the presence of the ICD band of the complex.[49] This seems plausible since dppz complexes show a strong electronic transition near 275 nm, which might interfere with the B-DNA band. If intercalation occurs with no specific orientation, the overlapping region will mimic the nucleobases stacking and a

dx.doi.org/10.1021/ic401067d | Inorg. Chem. 2013, 52, 8881−8894

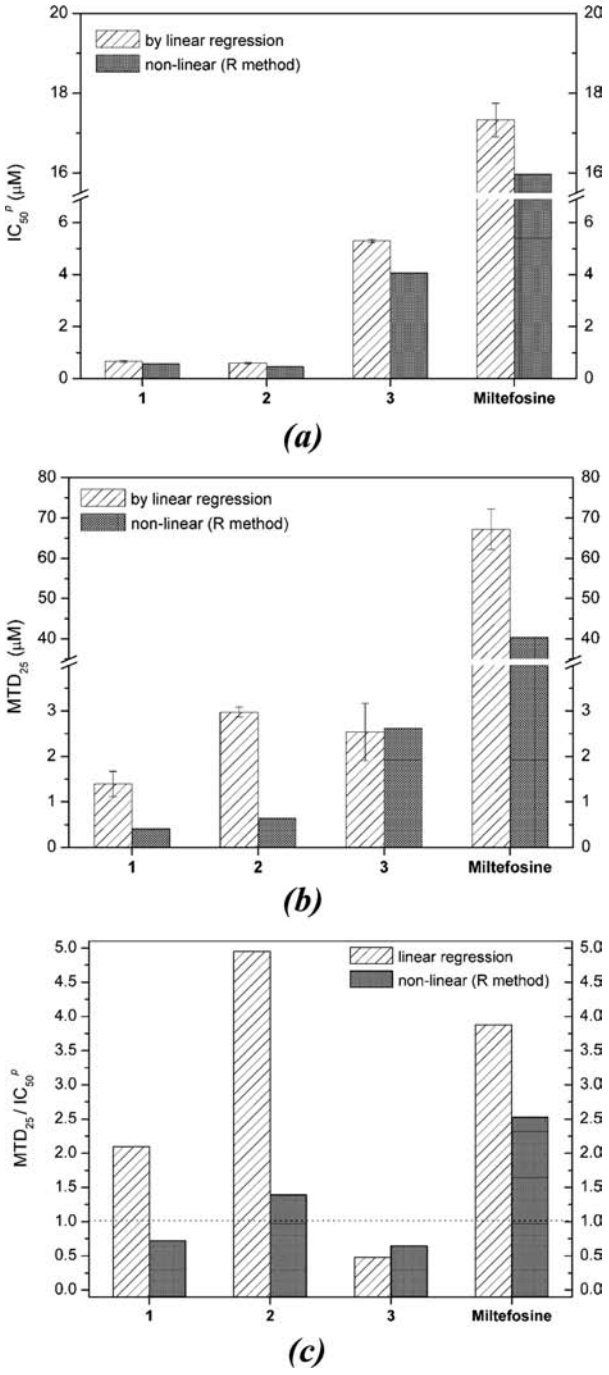

Figure 9. Susceptibility to compounds **1**–**3** and miltefosine: (a) IC_{50} for *L. infantum* (MHOM/PT/88/IMT-151) promastigotes (IC^{P}_{50}); (b) MTD_{25} for U937 macrophages; (c) MTD_{25}/IC^{P}_{50}. Graphics include average values and 2σ error margin for linear regression and average values for nonlinear *R* methodology.

positive increment is expected, while a change in sign might occur if extra interactions are able to position the intercalator with a specific orientation. While the presence of the negative ICD band at 275 nm in the spectra of B-DNA associated to **1** or **2** is a strong indication of a rigidified structure, since dppz is not particularly adequate to establish hydrogen bonds with the nucleobases (except for the phenazine nitrogen atoms), an alternative binding mode has to be found. One hypothesis is covalent binding since $[Ir(Cl)(Cp^*)(dppz)]^+$, where there is a 40% intensity reduction of (+) 270 nm at $R = 0.1$,[11] is known to bind DNA in such way. Similarly, $[FeCl_2(dppz)_2]Cl$, which rapidly interconverts to $[Fe(OH)_2(H_2O)(dppz)]$ in aqueous solutions, which is a much more adequate structure to coordinate to DNA nucleobases, has a CD that matches our observations with **1** and **2**.[47] For the present compounds, both pentacoordination, as seen in **1** in the solid state, or decoordination of one dppz, like previously observed in the iron compound, are alternatives to consider.

To understand the way the compounds interact with DNA, the evolution of ICD bands is as important as their wavelengths and sign. Figure 4b shows the normalized evolution of the band ca. 270 nm ($\Delta_{CD}/\Delta_{CD\infty}$) for both **1** and **2**. A sigmoidal profile is evident in both complexes, that is, they show a lag zone. Such behavior is consistent with two interaction modes, where only one of them causes changes in the band. The slope of the curve is sharper on **1** than **2**, indicating that on the last one the two modes coexist on a larger range of drug concentration. The amount of **2** needed to saturate DNA is approximately twice the amount of **1**. The lack of effect on CD for lower values of *R* indicates that the drugs should be initially present on the groove, most probably the major one taking into account the high stereochemical demand of the complexes, eventually with partial intercalation. Their accumulation gradually uncoils the DNA double helix, which then permits the complex to penetrate deeper in DNA and intercalate (cooperative effect). At higher *R* values a more rigid positioning of the complex might be the result of combined coordination and intercalation.

Contrary to compounds **1** and **2**, the Cu(I) complex, **3**, does not induce any change in DNA's CD spectrum, which indicates that it does not act as metallointercalator. Lack of characteristic ICD signals is not unusual for Cu(I) complexes, even when other studies confirm their ability to interact with DNA. An example is $[Cu(neo)_2]^+$ (neo = neocuproine) for which groove binding has been proposed.[50] Contrary to our results, Navarro et al. proposed that $[Cu(dppz)_2]BF_4$ is a good metallointercalator. Since $[Cu(dppz)_2]NO_3$ is barely soluble in aqueous buffers even with 20% v/v DMSO and nitrates are significantly more soluble than BF_4^-, both in water and in DMSO, a larger amount of DMSO should be necessary to guarantee its solubility. As we have shown in the present work, Cu(I)−dppz is easily oxidized by the presence of DMSO, strongly suggesting that a similar oxidation has occurred with $[Cu^{I}(dppz)_2]BF_4$. This seems to be confirmed by the lack of a band in the visible region of the published electronic spectrum of $[Cu^{I}(dppz)_2]BF_4$ in DMSO.[15] Furthermore, all biophysical and biological tests were performed under a large excess of chloride, which suggests that their results should come from $[CuCl(dppz)_2]Cl$ instead.

3.4.3. Rheometry. Hydrodynamic measurements that are sensitive to changes in molecular length, like viscosity, are considered less ambiguous tests to assign the interaction mechanism with DNA if no X-ray or NMR structures are available.[51] According to the classic model of intercalation, double-helix DNA length increases when the base pairs are separated to fit the intercalators among them, causing an increase in DNA solution viscosity.[52] Most of the classic monointercalators, like EtBr, obey the nearest neighbor exclusion principle, that is, "the occupation of a single intercalation site prevents subsequent intercalation both immediately 5′ and 3′ to the initial site" and show an increase in the viscosity that tends to evolve linearly until near saturation that occurs at a drug/DNA ratio (*R*) of 0.25.[53] Some other

dx.doi.org/10.1021/ic401067d | *Inorg. Chem.* 2013, 52, 8881−8894

Table 2. Parasite Susceptibility and Cell Viability Obtained for Complexes 1−3 and Miltefosine on the Promastigote and Amastigote Phases of *L. infantum* Strain and on the U-937 Human Macrophages Cell Line[a]

	linear regression					nonlinear regression (R methodology)				
compound	IC_{50}^{P}	MTD_{25}	MTD_{25}/IC_{50}^{P}	IC_{50}^{a}	MTD_{25}/IC_{50}^{a}	IC_{50}^{P}	MTD_{25}	MTD_{25}/IC_{50}^{P}	IC_{50}^{a}	MTD_{25}/IC_{50}^{a}
$[Cu(dppz)_2(CH_3COO)]$ CH_3COO, **1**	0.67 ± 0.03	1.39 ± 0.11	2.10	0.27 ± 0.02	5.08	0.57	0.41	0.72	na	
$[Zn(dppz)_2](BF_4)_2$, **2**	0.60 ± 0.07	2.98 ± 0.63	4.95	0.30 ± 0.03	9.89	0.46	0.64	1.39	0.26	2.51
$[Cu(dppz)_2]NO_3$, **3**	5.29 ± 0.04	2.54 ± 0.28	0.48			4.06	2.62	0.65		
miltefosine	17.33 ± 0.42	67.22 ± 5.00	3.88	11.02[b]	6.11	15.97	40.33	2.53	na	

[a]All concentration values in micromolar from the average of three independent and reproducible assays. IC_{50}^{a} and IC_{50}^{P} are the half-maximal inhibitory concentration in the amastigote and promastigote phases, respectively. MTD_{25} is the maximum tolerated dose, considered at acceptable loss cell of 25%. na, nonavailable, meaning that it was not possible to determine a converged value using the R methodology. [b]According to ref 70.

intercalators have DNA binding site sizes of three, four, or even five base pairs.[54]

Results for **1**−**3** and EtBr are indicated in Figure 5. Compounds **1** and **2** show a strong increase in viscosity and significantly are bigger than experiment by EtBr and **3** under the same conditions. While the first two complexes show a sigmoidal profile, DNA is much more easily saturated with **1** ($R \approx 0.10$) than with **2** ($R \approx 0.31$; extrapolated for 99% of the plateau value). These results indicate that neither **1** or **2** behaves as a classic intercalator. The sigmoidal profile suggests that at lower values of R there is an alternative mechanism to intercalation or at least some competition with it, probably external or groove binding, since it is known that such placements are characterized by no to small viscosity increases (limited uncoiling of the helix). The observed profiles indicate that the preference for intercalation or groove binding depends on the metal center. At low to moderate values of R, the viscosity increment caused by the Cu(II) compound is much bigger than the Zn(II) analogue, suggesting a better intercalation ability of the first. Such difference is most probably caused by the ease of the copper complex, compared to the zinc one, to accommodate the geometry distortions required for DNA binding, as seen in Figure 3. Nevertheless, since the global viscosity increment at the saturation point is almost the same, the equilibrium can be shifted to the intercalated form using an excess of compound. This same dual mechanism was recently proposed by Biver et al. to the related metallointercalator $[Ru(dppz)(phen)_2]^{2+}$,[55] where they noticed an accentuated positive cooperativity and salt concentration dependence, that is, an electrostatic contribution, at low values of R, supporting a groove-binding mode, while at $R > 0.22$ an intercalation process was observed.

While intercalation is well supported, a question remains. Why does complex **1** cause DNA saturation at such low concentration when there are supposedly still many intercalation sites available? One possibility is that DNA binding occurs simultaneously by covalent and noncovalent modes. To better evaluate it, we performed ESI-MS studies with GC oligomers, since they favor intercalation over other sequences with normal GC contents or AT rich (see section 3.4.5).

3.4.4. Atomic Force Microscopy. AFM studies were performed exclusively for compound **1** (Figure S5, Supporting Information) to determine its ability to change the length of circular plasmid DNA (l), which was measured with the program ImageJ 1.44p from NIH. The mica surface was modified to permit DNA immobilization. APTES was used instead of the standard 10 mM $MgCl_2$ since it was determined that the low concentration of complex (55.2 pM) cannot compete with Mg^{2+} for phosphate binding in DNA surface.

With APTES, complex **1** was shown to cover the circular plasmid DNA (perimeter). Data show an increase of ca. 8.5% with addition of the compound: $l = 0.892 \pm 0.015$ ($R = 0.000$), 0.968 ± 0.030 ($R = 0.125$), and 0.962 ± 0.029 nm ($R = 0.250$). These results are consistent with an intercalation interaction with DNA, with saturation occurring at $R \leq 0.125$, which agrees with CD and viscosity results.

While expanding the DNA length, addition of **1** does not cause an obvious change in the superhelicity (Figure S5, Supporting Information). This might be caused by a lower ability of APTES, when compared with Mg^{2+}, to unwind superhelical plasmid DNA.

3.4.5. QTof-ESI-MS of GC Oligonucleotides. The above-presented DNA biophysical studies support the ability of **1** and **2** to intercalate among the nucleobases and that there is a specific orientation of the complexes. Since the viscosity and CD titrations give sigmoidal profiles, a cooperative phenomenon is present and suggests groove accumulation previously to intercalation. Complex **1** has a bigger tendency to intercalate at lower complex:DNA ratio, which seems to be related with an increased distortion flexibility when compared to **2**. CD, rheometry, and AFM results consistently indicate that compound **1** saturates DNA at $R < 0.15$, while for **2** it only occurs at $R > 0.30$. Since dppz has no functional groups adequate to establish hydrogen bonds on the major groove, fixation of the structures, when intercalated, might come from an intercalation−coordination dual-binding mode. QTof-ESI-MS studies with oligonucleotides were conducted to get more details on the probable mechanism of interaction of the drugs. The electrospray ionization process is recognized as mild and able to keep intact in the gas phase the associations that occur in solution,[56] namely, the noncovalent ones between drugs and oligonucleotides.[57] This technique is also adequate to interpret association mechanisms since each binding mode has its own fragmentation signature. Studies of the interactions between **1**/**2** and GC oligonucleotides were conducted on the negative ion mode with *ds*(GCGCGCGC) and *ds*(GCGCGCGCGC), hereafter named 4GC and 5GC, respectively. On 4GC the most abundant ions have 3 and 4 negatives charges, while for 5GC the most abundant have 4 and 5. Choice of GC only sequences is intended to maximize the possibility of intercalation or major groove binding,[58] since AT-rich sequences tend to favor minor-groove binding,[59] based on adequate van der Waals contacts.[59c,60] Minor-groove binding in GC is unfavorable, because of the amine group of guanine,[58a,59b] but external binding and major groove are

dx.doi.org/10.1021/ic401067d | Inorg. Chem. 2013, 52, 8881−8894

possible, particularly when the drugs are able to form hydrogen bonds,[58a] or they are too big to adjust adequately as an intercalator.[61] A further reason for GC choice resides in CD studies with $[Fe(dppz)(phen)_2]^{2+}$. They show that the negative ICD band at 280−290 nm occurs only on ct-DNA and poly$[(dG-dC)_2]$ while poly$[(dA-dT)_2]$ results on a positive band at 275 nm.[62]

QTof-ESI-MS spectra of **1** or **2**, under experimental conditions similar to the ones used during this biophysical study, show that $[M(dppz)_2]^{2+}$ ions are stable. Therefore, the ions found on mixtures of the complexes with 4GC or 5GC indicate a change on the molecular structure of the complexes are caused by their association to the oligonucleotides.

When a drug interacts with oligonucleotides in a noncovalent way, MS/MS spectra of the double-strand ion, $[ds + Drug]^{n-}$, can show two characteristic patterns of fragmentation. One is $[ss]^{m-} + [ss + Drug]^{(n-m)-}$, characteristic of minor-groove binding, and the other is $[ds]^{m-} + [Drug]^{(n-m)-}$, observed in intercalators.[58c,63]

Compounds **1** and **2** show the same ion pattern for each oligonucleotide. The only noticeable difference resides in the fact that ions related with the copper compound are significantly more intense, and their spectra were chosen for representation. The m/z values of the more relevant ions observed during interaction of the complexes with the oligonucleotides are presented in Tables S2−S5, Supporting Information, the same as their assignments and predicted values. While discussion in this paper focuses on 4GC results, interactions with 5GC results in the same type of ions, with differences only on the respective m/z values (see Tables S4 and S5, Supporting Information).

Our first task during interpretation of the MS spectra was to find the ions that could be assigned to $[ds + x\{M(dppz)_2\}]^{3-/4-}$ or $[ds + x\{M(CH_3COO)(dppz)_2\}]^{3-/4-}$. None could be detected. Furthermore, the expected fragmentation ions for groove binding, $[ss + x\{M(dppz)_2\}]^{2-/3-}$ or $[ss + x\{M(CH_3COO)(dppz)_2\}]^{2-/3-}$, have not been found, while $[M(dppz)_2]^-$ or $[M(CH_3COO)(dppz)_2]^-$, which would be expected if classic intercalation occurs, are vestigial at best. Nevertheless, several secondary ions charged 3−/4− are observed at m/z values identical to $[ds + \{M(dppz)_2\} + yM]^{3-/4-}$ (y = 1−3) but none at m/z values equivalent to $[ds + x\{M(dppz)_2\}]^{3-/4-}$ or $[ss + \{M(dppz)_2\} + yM]^{2-/3-}$ (x, y = 1−3). In fact, the observed ions are the only ones that can also be formulated as a linear combination of {M(dppz)} and {M}. Thus, the ions are assigned instead to $[ds + x\{M(dppz) + yM\}]^{3-/4-}$ (x, y = 1−3 and $x + y \leq 4$). For 4GC and complex **1**, the diagnostic ions $[ds + x\{M(dppz) + yM\}]^{3-/4-}$ can be found in Figure 6 (a more expanded MS spectra can be found in Figure S6, Supporting Information). Among the many diagnostic ions, the more relevant include $[ds + Cu(dppz)]^{3-/4-}$ at m/z 1720/1290, $[ds + Cu(dppz) + Cu]^{3-/4-}$ at 1741/1305, and $[ds + 2Cu(dppz)]^{3-/4-}$ at 1835/1376. All proposed assignments fit quite well the theoretical isotope profile. As an example, the first two ions are given in Figure S7, Supporting Information.

More information can be taken from the tandem spectra of the diagnostic ions, obtained with modest collision energy to minimize fragmentation of 4GC. On such oligonucleotide, the 3− charged ions are less abundant than 4− and, consequently, their MS^2 spectra are not so well resolved. Nevertheless, they have no competing ions, contrary to 4−, which can suffer overlapping or be confused with single-strand 2− ions. MS^2 spectra for 1720 (3−) and 1835 (3−) ions are represented in Figures 7 and 8, respectively, while MS^2 spectra for ions 1290 (4−-) and 1376 (4−) can be found in the Supporting Information (Figures S8 and S9). All tandem spectra indicate that the main fragmentation process includes dppz loss with the copper ions remaining attached to 4GC, both in *ss* and *ds* forms. In the MS^2 of 1720 (3−) and 1835 (3−) it was possible to detect a low-abundant fragment ion at m/z 1606, eventually $[ds]^{3-}$, which suggests that, at best, just a small fraction of the complex might be only intercalated, instead of the dual-association mode that is proposed as the main fragmentation process. Furthermore, no signs of $[ss + x\{Cu(dppz)\}]^{(n-m)-}$ fragment ions were observed in such MS^2 spectra, as would be expected if groove binding was the main mechanism. In fact, many other MS^2 spectra of $[ds + x\{Cu(dppz) + yCu\}]^{3-/4-}$ diagnostic ions were acquired, and they all indicate that the major fragmentation process includes loss of the second dppz instead of formation of $[ss + x\{Cu(dppz) + yCu\}]^{2-}$, which excludes groove binding as a significant alternative. The fact that a few ions that might correspond to $[ss + x\{Cu(dppz)\}]^{n-}$ were detected on the MS spectra is probably the result of association of the complexes to *ss* in solution, with the compounds having a strong preference for *ds* over *ss*. Two of these ions appear at 917 (3−) and 1376 (2−) (see Figures S10 and S11, Supporting Information).

Many *ss* and *ds* ions associated to metal cations, like $[ds + yCu]^{3-/4-}$ and $[ss + yCu]^{2-/3-}$, are very abundant (Figure S6a,b, Supporting Information) despite the very mild experimental conditions used on MS experiments. Further support for the proposed assignments comes from experiments with 4GC and copper acetate that show exactly the same associated ions, isotope profile, and MS^2 fragmentations. The abundance of such MS ions indicates that not only they are expected to result from gas phase fragmentation of $[ds + x\{Cu(dppz) + yCu\}]^{3-/4-}$ ions but that a coordination sphere evolution should occur in solution after binding to the oligonucleotides with successive losses of coordinated dppz's that should be replaced by covalent binding to GC.

Summarizing, the more characteristic ions from association of **1** and **2** with 4GC and 5GC correspond to $[ds + x\{Cu(dppz)\} + yCu]^{3-/4-}$ and $[ds + yCu]^{3-/4-}$. The most probable mechanism of the drugs association to 4GC/5GC is the one where binding is preceded by loss of dppz followed by intercalation and covalent binding. The fact that no dppz loss occurs in solvated complexes ($[M(dppz)_2]^{2+}$) but that it takes place when the compounds interact with DNA can be a consequence of the stereochemical hindrance between $[M(dppz)_2]^{2+}$ and the double helix (or between accumulated $[M(dppz)_2]^{2+}$ molecules in the major groove). Such interactions will increase the energy of the compound and, simultaneously, decrease the energy barrier to dppz loss. Intercalation and covalent binding to nucleobases should overcome the energy required to loss of a dppz unit. Even if enthalpy favors $\{M(dppz)_2\}$, the nonequilibrium system is biased toward maximum instantaneous entropy production[64] that occur with {[M(dppz)] + dppz}. The dissociated dppz will hardly be able to bind the metal again, while DNA sites are always available.

3.5. Leishmanicidal Activity and Cytotoxicity. We decided to study the leishmanicidal activity of complexes **1** and **2** since it is known that compounds able to interact with DNA have a good probability to be antiprotozoal drugs.[65] Previously, Navarro and collaborators[14k,15] prepared two

dx.doi.org/10.1021/ic401067d | Inorg. Chem. 2013, 52, 8881−8894

Cu(II) compounds, $[Cu(NO_3)(dppz)]NO_3$ and $[Cu(NO_3)(dppz)_2]NO_3$, and a Cu(I) analogue, $[Cu^I(dppz)_2]BF_4$, which are active against some *Leishmania* strains known to cause the cutaneous form of the disease. Meanwhile, no such effect was seen for ionic forms of copper, and dppz alone was much less active than the complexes (IC_{25} = 10 μM). On the basis of biophysical experiments (agarose gel and viscosity studies, spectroscopic titrations of DNA) and ultrastructural studies (TEM of promastigotes) they proposed that DNA is a cellular target for the drugs. They tested only the sensitivity of the promastigote form of the parasite. In vitro studies with parasite cultures are common, but promastigotes studies have limited medical relevance.[66] Only the intracellular phase corresponds to an adequate model to correlate the results with an in vivo response to treatment, particularly when evaluating resistance phenomena.[67] We decided to evaluate the cellular toxicity of **1** and **2** in human macrophages and the sensitivity of the amastigote form of the parasite in infected cells, since such studies had not been previously performed for Cu−dppz compounds and would permit us to determine the compounds therapeutic index. *L. infantum* was the selected strain in all tests because it is known to cause the more dangerous form of the disease, visceral leishmaniasis.

Compound **2** is the first Zn−dppz compound to be studied, despite the fact that lower levels of zinc are characteristic in human leishmaniasis, suggesting therapeutic administration, and their compounds are expected to be less toxic to human cells than the copper analogues.[17−19] A strategy based on combination of an essential metal with a ligand that typically results in good metallointercalators can be seen as an extension of the concept of *poison and bait combined strategy*, well known in ferrocenyl derivatives developed to treat malaria.[68]

The viability of cells/microorganisms versus the amount of drugs, given on a logarithmic scale, was determined by two different methodologies. The first corresponds to the common linearization method, while the second is a nonlinear approach, named R methodology, already described in the Experimental Section (section 2.4). Introduction of a more complex approach resulted from the lack of linearity that copper and zinc compounds showed on both the half-maximal inhibitory concentration, IC_{50}, determined in *L. infantum* parasites, and the maximum tolerated dose, MTD_{25}, evaluated in U-937 macrophages host cells. Results of both methodologies are presented in Figure 9 and Table 2. With one exception only, values of IC_{50} and MTD_{25} obtained with the R methodology are smaller than the ones obtained with the linearization process. Except where indicated, IC_{50} and MTD_{25} values refer to the nonlinear approach.

Compounds **1**/**2** are more active (IC_{50}) against the promastigote form of *L. infantum* (0.46−0.57 μM) than miltefosine (16 μM), but they are also more cytotoxic to human cells (0.41−0.64 μM vs 40.33 μM for miltefosine). The Cu(II) compound (**1**) is 6−7 times more active and cytotoxic than its Cu(I) analogue (**3**). Interchangeable Cu(I)/Cu(II) oxidation states are known to occur in solutions of **1** and **3**, but the lower charge of Cu(I) will decrease the electrostatic interaction with DNA. Intercalation between nucleobases seems to have major relevance on *L. infantum* promastigotes susceptibility, since the Zn(II) complex, **2**, lacking redox activity, is at least as active as the Cu(II) compound, **1**, and both are more active than **3**, which apparently is not a good intercalator. Nuclease and/or hydrolase activity, as seen in other Cu(II)−dppz complexes,[14j,36,69] is a plausible explanation for the increased cytotoxicity of **1** compared with **2**.

Linear regression data show that there is an improvement on IC_{50} results of **1**/**2** and the control miltefosine when changing the study to the amastigote phase. There is a consequent increase of the therapeutic index ($MTD_{25}/IC_{50}{}^a$) showing that nontoxic pharmaceuticals for leishmaniasis treatment might be developed with metal complexes. It was still possible to determine $IC_{50}{}^a$ for compound **2** using the nonlinear methodology (0.26 μM). A significant decrease in the value of MTD_{25} by the nonlinear method results in a worse therapeutic index than the one obtained by linear regression (9.89 vs 2.51) but still significantly high.

4. CONCLUSIONS

Compounds $[Cu(CH_3COO)(dppz)_2]CH_3COO$, **1**, and $[Zn(dppz)_2](BF_4)_2$, **2**, have been synthesized and characterized in the solid state and solution. Their interaction with DNA was studied by thermal denaturation, CD, rheometry, and AFM, while QTof-ESI-MS^- was applied for the study with GC oligonucleotides. Combined data indicate that the compounds behave as nonclassic metallointercalators with a cooperative interaction. The complexes probably accumulate on the surface or major groove up to a threshold (the viscosity and CD profiles indicate a lag phase at lower *R* values), after which they migrate to the intercalation site. Such step must be preceded or occur in a concerted manner with dppz loss and covalent binding to nucleobases (as seen by mass spectrometry). While the mechanism is the same, the threshold for the copper compound is lower than the zinc one. According to molecular modeling results, it seems that such difference is caused by the increased flexibility of the copper compound to distort its geometry, permitting easier penetration of DNA. Despite the fact that only one dppz remains attached to the metal cation when bound to DNA, the original formula where two dppz's are bound should correspond to more active compounds, since it will minimize the chance of their inactivation by covalent binding to alternative targets. As an example, $[Cu(NO_3)(dppz)_2]^{2+}$ has proved to be more active against *L. braziliensis* promastigotes than $[Cu(NO_3)(dppz)]^{2+}$ (ref 14k).

Compounds **1** and **2** are active against promastigotes and amastigotes of the *L. infantum* strain at submicromolar dosage, but **2** gave a better therapeutic index, even higher than the reference drug miltefosine. The fact that the redox-inactive zinc complex is as active as the copper compound supports an antileishmanial activity mechanism based on DNA interaction ability. This is reinforced with the observation that the Cu(I) complex **3**, $[Cu(dppz)_2]NO_3$, which showed no signs of DNA intercalation, was significantly less active than its Cu(II) analogue **1**.

While more active than the control miltefosine, compounds **1** and **2** are also more cytotoxic on U937 macrophage cells, particularly the copper complex. The action of this last compound is probably due to a combination of DNA intercalation and free radicals induction (hydroxyl and/or singlet oxygen) as seen in other copper−dppz complexes identified as synthetic nucleases and hydrolases.[14j,36,69]

■ ASSOCIATED CONTENT

Ⓢ Supporting Information

Spectroscopic characterization of complexes (infrared and UV−vis), thermal denaturation, AFM images, and ESI-MS studies of complexes:DNA interactions, generalized additive model charts

dx.doi.org/10.1021/ic401067d | Inorg. Chem. 2013, 52, 8881−8894

of macrophages and parasite cells viability, and coordinates of energy-minimized structure of the complexes. This material is available free of charge via the Internet at http://pubs.acs.org.

AUTHOR INFORMATION

Corresponding Author

*E-mail: jlmadureira@vcu.edu.

Present Address

[§]Departamento de Química Fundamental, Instituto de Química, Universidade de São Paulo, P.O. Box 26077, CEP 05513-970, São Paulo, SP, Brazil.

Notes

The authors declare no competing financial interest.

ACKNOWLEDGMENTS

We thank Fundação para a Ciência e a Tecnologia (FCT), Portugal, for providing financial (EU/FEDER POCI 2010 project PTDC/QUI/72656/2006) and fellowship support (J.M. (SFRH/BPD/41138/2007), C.M. (SFRH/BPD/44082/2008), and C.R. (SFRH/BD/30755/2006)). The authors wish to acknowledge AEterna Zentaris, Inc. (Germany) for providing miltefosine. J.M. thanks Dr. Fernando Santos (FCUL) for assistance on rheometry studies.

REFERENCES

(1) Jamieson, E. R.; Lippard, S. J. *Chem. Rev.* **1999**, *99*, 2467−2498.

(2) (a) Orkey, N.; Wormell, P.; Aldrich-Wright, J. *Metallointercalators, Synthesis and Techniques to Probe Their Interactions with Biomolecules*; Aldrich-Wright, J., Ed.; Springer: Wien and New York, 2011, pp 27−67. (b) Liu, H.-K.; Sadler, P. J. *Acc. Chem. Res.* **2011**, *44*, 349−359. (c) Browne, W. R.; McGarvey, J. J. *Coord. Chem. Rev.* **2006**, *250*, 1696−1709. (d) Cusumano, M.; Di Petro, M. L.; Giannetto, A. *Inorg. Chem.* **2006**, *45*, 230−235. (e) Lu, W.; Vicic, D. A.; Barton, J. K. *Inorg. Chem.* **2005**, *44*, 7970−7980. (f) Sastri, C. V.; Mariappan, M.; Ghosh, T.; Maiya, B. G. *Proc. Indian Natl. Sci. Acad. A* **2004**, *70*, 355−365. (g) Zou, X.-H.; Ji, L.-N. *Trends Inorg. Chem.* **2001**, *7*, 99−107. (h) Erkkila, K. E.; Odom, D. T.; Barton, J. K. *Chem. Rev.* **1999**, *99*, 2777−2796. (i) Che, C.-M.; Yang, M.; Wong, K.-H.; Chan, H.-L.; Lam, W. *Chem.—Eur. J.* **1999**, *5*, 3350−3356.

(3) (a) Benedetti, B. T.; Peterson, E. J.; Kabolizadeh, P.; Martinez, A.; Kipping, R.; Farrell, N. P. *Mol. Pharmaceutics* **2011**, *8*, 940−948. (b) Ruiz, J.; Vicente, C.; de Haro, C.; Espinosa, A. *Inorg. Chem.* **2011**, *50*, 2151−2158. (c) Gao, E.; Zhu, M.; Yin, H.; Liu, L.; Wu, Q.; Sun, Y. *J. Inorg. Biochem.* **2008**, *102*, 1958−1964. (d) Wheate, N. J.; Brodie, C. R.; Collins, J. G.; Kemp, S.; Aldrich-Wright, J. R. *Mini-Rev. Med. Chem.* **2007**, *7*, 627−648. (e) Baruah, H.; Bierbach, U. *J. Biol. Inorg. Chem.* **2004**, *9*, 335−344. (f) Baruah, H.; Barry, C. G.; Bierbach, U. *Curr. Top. Med. Chem.* **2004**, *4*, 1537−1549. (g) Barnes, K. R.; Lippard, S. J. *Metal Complexes in Tumor Diagnosis and as Anticancer Agents*; Sigel, A., Sigel, H., Eds.; Metal Ions in Biological Systems; Marcel Dekker: New York, 2004; Vol. *42*, pp 143−177.

(4) (a) Bruijnincx, P. C. A.; Sadler, P. J. *Curr. Opin. Chem. Biol.* **2008**, *12*, 197−206. (b) Bugarcic, T.; Novakova, O.; Halamikova, A.; Zerzankova, L.; Vrana, O.; Kasparkova, J.; Habtemariam, A.; Parsons, S.; Sadler, P. J.; Brabec, V. *J. Med. Chem.* **2008**, *51*, 5310−5319.

(5) (a) De Pascali, S. A.; Migoni, D.; Papadia, P.; Romano, A.; Marsigliante, S.; Pellissier, A.; Chardon-Noblat, S.; Ciccarese, A.; Fanizzi, F. P. *Dalton Trans.* **2008**, 5911−5921. (b) Petitjean, A.; Barton, J. K. *J. Am. Chem. Soc.* **2004**, *126*, 14728−14729.

(6) Gencaslan, S.; Sheldrick, W. S. *Eur. J. Inorg. Chem.* **2005**, 3840−3849.

(7) Farrell, N. *Met. Ions Biol. Syst.* **1996**, *32*, 603−639.

(8) Yan, Y. K.; Melchart, M.; Habtemariam, A.; Sadler, P. J. *Chem. Commun.* **2005**, 4764−4776.

(9) Ma, Z.; Choudhury, J. R.; Wright, M. W.; Day, C. S.; Saluta, G.; Kucera, G. L.; Bierbach, U. A. *Cancer J. Med. Chem.* **2008**, *51*, 7574−7580.

(10) Milkevitch, M.; Shirley, B. W.; Brewer, K. J. *Inorg. Chim. Acta* **1997**, *264*, 249−256.

(11) Schäfer, S.; Sheldrick, W. S. *J. Organomet. Chem.* **2007**, *692*, 1300−1309.

(12) Smith, S. R.; Neyhart, G. A.; Kalsbeek, W. A.; Thorp, H. H. *New J. Chem.* **1994**, *18*, 397−406.

(13) Gosh, S.; Barve, A. C.; Kumbhar, A. A.; Kumbhar, A. S.; Puranik, V. G.; Datar, P. A.; Sonawane, U. B.; Joshi, R. R. *J. Inorg. Biochem.* **2006**, *100*, 331−343.

(14) (a) Chen, G.-J.; Qiao, X.; Qiao, P.-Q.; Xu, G.-J.; Xu, J.-Y.; Tian, J.-L.; Gu, W.; Liu, X.; Yan, S.-P. *J. Inorg. Biochem.* **2011**, *105*, 119−126. (b) Hong, J.; Li, X.-Y.; Weng, Ng, S. . *Acta Crystallogr., Sect. E: Struct. Rep. Online* **2011**, *67*, m1322. (c) Li, X.; Liu, C.; Che, G.; Wang, X.; Li, C.; Yan, Y.; Guan, Q. *Inorg. Chim. Acta* **2010**, *363*, 1359−1366. (d) Ramakrishnan, S.; Palaniandavar, M. *Dalton Trans.* **2008**, 3866−3878. (e) Wang, X.-Y.; Wang, J.-J.; Ng, S. W. *Acta Crystallogr., Sect. C: Cryst. Struct. Commun.* **2008**, *64*, m401−m404. (f) Roy, M.; Pathak, B.; Patra, A. K.; Jemmis, E. D.; Nethaji, M.; Chakravarty, A. R. *Inorg. Chem.* **2007**, *46*, 11122−11132. (g) Zhou, F.-C.; Fang, W.; Dong, E.-J.; Li, C.-B. *Acta Crystallogr., Sect. E: Struct. Rep. Online* **2007**, *63*, m660−m661. (h) Zhang, S.-Cai; Sun, J. *Acta Crystallogr., Sect. E: Struct. Rep. Online* **2006**, *62*, m3107−m3109. (i) Thomas, A. M.; Nethaji, M.; Chakravarty, A. R. *J. Inorg. Biochem.* **2004**, *98*, 1087−1094. (j) Gupta, T.; Dar, S.; Nethaji, M.; Chakravarty, A. R. *Dalton Trans.* **2004**, 1896−1900. (k) Navarro, M.; Cisneros-Fajardo, E. J.; Sierralta, A.; Fernandez-Mestre, M.; Silva, P.; Arrieche, D.; Marchan, E. *J. Biol. Inorg. Chem.* **2003**, *8*, 401−408. (l) Santra, B. K.; Reddy, A. N.; Neelakanta, G.; Mahadevan, S.; Nethaji, M.; Chakravarty, A. R. *J. Inorg. Biochem.* **2002**, *89*, 191−196.

(15) Navarro, M.; Cisneros-Fajardo, E. J.; Fernandez-Mestre, M.; Arrieche, D.; Marchan, E. *J. Inorg. Biochem.* **2003**, *97*, 364−369.

(16) *Control of the Leishmaniasis: Report of the WHO Expert Committee on the Control of Leishmaniases*; World Health Organization: WHO Press, Geneva, Switzerland, 2010.

(17) Pasa, S.; Kargin, F.; Bildik, A.; Seyrek, K.; Ozbel, Y.; Ozensoy, S. *Biol. Trace Elem. Res.* **2003**, *94*, 141−147.

(18) van Weyenbergh, J.; Santana, G.; D'Oliveira, A.; Santos, A. F.; Costa, C. H.; Carvalho, E. M.; Barral, A.; Barral-Netto, M. *BMC Infect. Dis.*, **2004**, *4*, 50.

(19) Sharquie, K. E.; Najim, R. A.; Farjon, I. B.; Al-Timimi, D. J. *Clin. Exp. Dermatol.* **2001**, *26*, 21−26.

(20) Alvar, J.; Croft, S.; Olliaro, P. *Adv. Parasitol.* **2006**, *61*, 223−274.

(21) Dujardin, J. C.; González-Pacanowska, D.; Croft, S. L.; Olesen, O. F.; Späth, G. F. *Trends Parasitol.* **2010**, *26*, 395−403.

(22) Frisch, M. J.; Trucks, G. W.; Schlegel, H. B. et al. *Gaussian 03*, Revision D.02; Gaussian, Inc.: Wallingford, CT, 2004. See Supporting Information for full citation.

(23) Becke, A. D. *Phys. Rev. A* **1988**, *38*, 3098−3100.

(24) Lee, C.; Yang, W.; Parr, R. G. *Phys. Rev. B* **1988**, *37*, 785−789.

(25) Zhurko, G. A. *Chemcraft*, v. 1.6; http://www.chemcraftprog.com.

(26) PyMOL Incentive Product, DeLano Scientific LLC (2006). The PyMOL Executable Build incorporates Open-Source PyMol 0.99rc6.

(27) (a) Felsenfeld, G.; Hirschman, S. Z. J. *J. Mol. Biol.* **1965**, *13*, 407−427. (b) Reichmann, M. E.; Rice, S. A.; Thomas, C. A.; Doty, P. *J. Am. Chem. Soc.* **1954**, *76*, 3047−3053.

(28) Marmur, J. *J. Mol. Biol.* **1961**, *3*, 208−218.

(29) Ramos, C. I. V. Estudo de aductos não covalentes de porfirinas com oligonucleótidos por espectrometria de massa. Master Thesis; Universidade de Aveiro: Aveiro, Portugal, 2005.

(30) Ramos, C. I. V.; Barros, C. M.; Fernandes, A. M.; Santana-Marques, M. G.; Ferrer Correia, A. J.; Tomé, J. P. C.; Carrilho, M. C. T.; Faustino, M.; Amparo, F.; Tomé, A. C.; Neves, M. G. P. M. S.; Cavaleiro, J. A. S. *J. Mass Spectrom.* **2005**, *40*, 1439−1447.

(31) Maia, C.; Rolão, N.; Nunes, M.; Gonçalves, L.; Campino, L. *Acta Trop.* **2007**, *103*, 150−155.

(32) Williams, C.; Espinosa, O.; Montenegro, H.; Cubilla, L.; Capson, T. L.; Ortega-Barria, E.; Romero, L. I. *J. Microbiol. Methods* **2003**, *55*, 813−816.
(33) R Development Core Team. *R: A language and environment for statistical computing*; R Foundation for Statistical Computing: Vienna, Austria, 2010; http://www.R-project.org.
(34) Dickeson, J. E.; Summers, L. A. *Aust. J. Chem.* **1970**, 1023−1027.
(35) Madureira, J.; Proença, L.; Crespo, O.; Madeira, P.; Fonseca, I.; Laguna, A.; Florêncio, H.; Farrell, N.; Calhorda., M. J. Manuscript in preparation.
(36) Ameerunisha Begum, M. S.; Saha, S.; Hussain, A.; Chakravarty, A. R. *Indian J. Chem.* **2009**, *48A*, 9−14.
(37) Nakamoto, K. *Infrared and Raman Spectra of Inorganic and Coordination Compounds, Part B: Applications in Coordination, Organometallic and Bioinorganic Chemistry*, 5th ed.; John Wiley & Sons: New York, 1997; pp 59−60.
(38) Hadadzadeha, H.; Fatemi, S. J. A.; Hosseinian, S. R.; Khavasi, H. R.; Pöttgen, R. *Polyhedron* **2008**, *27*, 249−254.
(39) (a) An, Y.; Li, X.-F.; Dong, L.-H.; Yin, Y.-S. *Acta Crystallogr., Sect. E: Struct. Rep. Online* **2008**, *64*, m1291−m1292. (b) Che, G.-B.; Xu, Z.-L.; Liu, C.-B. *Acta Crystallogr., Sect. E: Struct. Rep. Online* **2006**, *62*, m1695−m1696.
(40) (a) Liu, C.-B.; Gao, L.; Li, X.-Y.; Xu, Z.-L.; Wang, Q.-W.; Che, G.-B. *Chin. J. Struct. Chem.* **2011**, *30*, 262−266. (b) Wang, X.-F. *Acta Crystallogr., Sect. E: Struct. Rep. Online* **2011**, *67*, m447. (c) Han, Z.-B.; Ji, J.-W.; An, H.-Y.; Zhang, W.; Han, G.-X.; Zhang, G.-X.; Yang, L.-G. *Dalton Trans.* **2009**, 9807−9811.
(41) (a) Jing, B.; Li, L.; Dong, J.; Xu, T. *Acta Crystallogr., Sect. E: Struct. Rep. Online* **2011**, *67*, m464. (b) Tu, B.-T.; Xie, H.-Z.; Rena, Y.-T.; Chen, J.-Z. *Acta Crystallogr., Sect. E: Struct. Rep. Online* **2008**, *64*, m1475. (c) Xu, W.; Lin, J.-L.; Xie, H.-Z.; Zhang, M. *Acta Crystallogr., Sect. E: Struct. Rep. Online* **2008**, *64*, m1496. (d) Barceló-Oliver, M.; García-Raso, Á.; Terrón, Á.; Molins, E.; Prieto, M. J.; Moreno, V.; Martínez, J.; Lladó, V.; López, I.; Gutiérrez, A.; Escribá, P. V. *J. Inorg. Biochem.* **2007**, *101*, 649−659. (e) Zheng, Y.-Q.; Sun, J.; Lin, J.-L. *Z. Anorg. Allg. Chem.* **2001**, *627*, 90−94.
(42) Wang, J.; Jin, Z. *Acta Crystallogr., Sect. E: Struct. Rep. Online* **2010**, *66*, m865 . While the authors say that acetate in $[Cu(CH_3COO)(phen)_2]CF_3COO$ binds in a bidentate mode, their X-ray indicates the same type of square pyramidal geometry with the noncoordinated oxygen atom of acetate at a bigger distance from the copper center (ca. 2.7 Å) and significantly deviated from the axial orientation (148°), like in other k^1-RCOO structures..
(43) Nikolova, D.; Georgiev, M. *J. Therm. Anal. Calorim.* **2009**, *95*, 319−321.
(44) Munoz-Hernandez, M.-A.; Keizer, T. S.; Wei, P.; Parkin, S.; Atwood, D. A. *Inorg. Chem.* **2001**, *40*, 6782−6787.
(45) Minenkov, Y.; Singstad, Å.; Occhipinti, G.; Jensen, V. R. *Dalton Trans.* **2012**, *41*, 5526−5541.
(46) Nordén, B.; Tjerneld, F. *Biopolymers* **1982**, *21*, 1713−1734.
(47) Terenzi, A.; Barone, G.; Silvestri, A.; Giuliani, A. M.; Ruggirello, A.; Turco Liveri, V. *J. Inorg. Biochem.* **2009**, *103*, 1−9.
(48) (a) Bieda, R.; Dobroschke, M.; Triller, A.; Ott, I.; Spehr, M.; Gust, R.; Prokop, A.; Sheldrick, W. S. *ChemMedChem* **2010**, *5*, 1123−1133. (b) Chen, L.-M.; Liu, J.; Chen, J.-C.; Tan, C.-P.; Shi, S.; Zheng, K.-C.; Ji, L.-N. *J. Inorg. Biochem.* **2008**, *102*, 330−341. (c) González, V. M.; Amo-Ochoa, P.; Pérez, J. M.; Fuertes, M. A.; Masaguer, J. R.; Navarro-Ranninger, C.; Alonso, C. *J. Inorg. Biochem.* **1996**, *63*, 57−68.
(49) Dalgleish, D. G.; Fujita, H.; Peacock, A. R. *Biopolymers* **1969**, *8*, 633−645. (b) Dalgleish, D. G.; Peacocke, A. R.; Fey, G.; Harvey, C. *Biopolymers* **1971**, *10*, 1853−1863.
(50) (a) Liu, F.; Meadows, K. A.; McMillin, D. R. *J. Am. Chem. Soc.* **1993**, *115*, 6699−6704. (b) Tamilarasan, R.; McMillin, D. R. *Inorg. Chem.* **1990**, *29*, 2798−2802. (c) Graham, D. R.; Sigman, D. S. *Inorg. Chem.* **1984**, *23*, 4188−4191.
(51) (a) Satyanarayana, S.; Dabrowiak, J. C.; Chaires, J. B. *Biochemistry* **1993**, *32*, 2573−2584. (b) Satyanarayana, S. J.; Dabrowiak, C.; Chaires, J. B. *Biochemistry* **1992**, *31*, 9319−9324.
(52) Lerman, L. S. *J. Mol. Biol.* **1961**, *3*, 18−30.
(53) (a) Kobertz, W. R.; Wang, D.; Wogan, G. N.; Essigmann, J. M. *Proc. Natl. Acad. Sci. U.S.A.* **1997**, *94*, 9579−9584. (b) Wilson, W. D. In *Nucleic acids in Chemistry and Biology*; Blackburn, G. M., Gait, M. J., Eds.; Oxford University Press: New York, 1990; pp 295−336. (c) Crothers, D. M. *Biopolymers* **1968**, *6* (4), 575−584.
(54) Rosu, F.; Pirotte, S.; De Pauw, E.; Gabelica, V. *Int. J. Mass Spectrom.* **2006**, *253*, 156−171.
(55) Biver, T.; Cavazza, C.; Secco, F.; Venturini, M. *J. Inorg. Biochem.* **2007**, *101*, 461−469.
(56) Gaskell, S. J. *J. Mass. Spectrom.* **1997**, *32*, 677−688.
(57) (a) Gabelica, V.; De Pauw, E. *Int. J. Mass. Spectrom.* **2002**, *219*, 151−159. (b) Gabelica, V.; De Pauw, E. *J. Mass. Spectrom.* **2001**, *36*, 397−402. (c) Loo, J. A.; Sannes-Lowery, K. A.; Hu, P.; Mack, D. P.; Mei, H.-Y. *NATO ASI Ser., Ser. C* **1998**, *510*, 83−99. (d) Gao, Q.; Cheng, X.; Smith, R. D.; Yang, C. F.; Goldberg, I. H. *J. Mass Spectrom.* **1996**, *31*, 31−36. (e) Gale, D. C.; Smith, R. D. *J. Am. Soc. Mass Spectrom.* **1995**, *6*, 1154−1164. (f) Hsieh, Y. L.; Li, Y. T.; Henion, J. D.; Ganem, B. *Biol. Mass Spectrom.* **1994**, *23*, 272−276. (g) Gale, D. C.; Goodlett, D. R.; Light-Wahl, K. J.; Smith, R. D. *J. Am. Chem. Soc.* **1994**, *116*, 6027−6028.
(58) (a) Bischoff, G.; Hoffmann, S. *Curr. Med. Chem.* **2002**, *9*, 312−348. (b) Lisgarten, J. N.; Coll, M.; Portugal, J.; Wright, C. W.; Aymami, J. *Nat. Struct. Biol.* **2002**, *9*, 57−60. (c) Wan, K. W.; Shibue, T.; Gross, M. L. *J. Am. Chem. Soc.* **2000**, *122*, 300−307. (d) Geierstanger, B. J.; Wemmer, D. E. *Annu. Rev. Biophys. Biomol. Struct.* **1995**, *24*, 463−493. (e) Nandi, R.; Chakraborty, S.; Maiti, M. *Biochemistry* **1991**, *30*, 3715−3720.
(59) (a) Neidle, S. *Nat. Prod. Rep.* **2001**, *18*, 291−309. (b) Ren, J.; Chaires, J. B. *Biochemistry* **1999**, *38*, 16067−16075. (c) Neidle, S.; Nunn, C. M. *Nature Prod. Rep.* **1998**, *15*, 1−15.
(60) Wemmer, D. E. *Annu. Rev. Biophys. Biomol. Struct.* **2000**, *29*, 439−461.
(61) Kim, H.-K.; Lincoln, P.; Nordén, B.; Tuite, E. *Chem. Commun.* **1997**, 2375−2376.
(62) Mudasir, K.; Wijaya, E. T.; Wahyuni, H.; Inoue, N.; Yoshioka. *Spectrochim. Acta, Part A* **2007**, *66*, 163−170.
(63) (a) Gabelica, V.; De Pauw, E. *J. Am. Soc. Mass Spectrom.* **2002**, *13*, 91−98. (b) Wan, K. W.; Gross, M. L.; Shibue, T. *J. Am. Soc. Mass Spectrom.* **2000**, *11*, 450−457. (c) Gabelica, V.; De Pauw, E.; Rosu, F. *J. Mass Spectrom.* **1999**, *34*, 1328−1337.
(64) Wissner-Gross, A. D.; Freer, C. E. *Phys. Rev. Lett.* **2013**, *110*, 168702 and references therein.
(65) Wilson, W. D.; Tanious, F. A.; Mathis, A.; Tevis, D.; Hall, J. E.; Boykin, D. W. *Biochimie* **2008**, *90*, 999−1014.
(66) Sharief, A.; Khalil, E.; Theander, T.; Kharazmi, A.; Omer, S.; Ibrahim, M. *Exp. Parasitol.* **2006**, *114*, 247−252.
(67) (a) Croft, S.; Sundar, S.; Fairlamb, A. *Clin. Microbiol. Rev.* **2006**, *19*, 111−126. (b) Lira, R.; Sundar, S.; Makharia, A.; Kenney, A.; Gam, A.; Saraiva, E.; Sacks, D. *J. Infect. Dis.* **1999**, *180*, 564−567. (c) Ibrahim, M.; Hag, M.; El-Hassan, A.; Theander, T.; Kharazmi, A. *Parasitol. Res.* **1994**, *80*, 569−574.
(68) (a) Atteke, C.; Ndong, J. M.; Aubouy, A.; Maciejewski, L.; Brocard, J.; Lebibi, J.; Deloron, P. *J. Antimicrob. Chemother.* **2003**, *51*, 1021−1024. (b) Pradines, B.; Tall, A.; Rogier, C.; Spiegel, A.; Mosnier, J.; Marrama, L.; Fusai, T.; Millet, P.; Panconi, E.; Trape, J. F.; Parzy, D. *Trop. Med. Int. Health* **2002**, *7*, 265−270. (c) Pradines, B.; Fusai, T.; Daries, W.; Laloge, V.; Rogier, C.; Millet, P.; Panconi, E.; Kombila, M.; Parzy, D. *Antimicrob. Agents Chemother.* **2001**, *48*, 179−184. (d) Chibale, K.; Moss, J. R.; Blackie, M.; van Schalkwyk, D.; Smith, P. J. *Tetrahedron Lett.* **2000**, *41*, 6231−6235. (e) Biot, C.; Glorian, G.; Maciejewski, L. A.; Brocard, J. S.; Domarle, O.; Blampain, G.; Millet, P.; Georges, A. J.; Abessolo, H.; Dive, D.; Lebibi, J. *J. Med. Chem.* **1997**, *40*, 3715−3718.
(69) Thomas, A. M.; Nethaji, M.; Mahadevan, S.; Chakravarty, A. R. *J. Inorg. Biochem.* **2003**, *94*, 171−178.
(70) Maia, C. S. Interacção Parasita-Hospedeiro e susceptibilidade de Leishmania infantum a fármacos. Ph.D. Thesis, Universidade Nova de Lisboa, Portugal, 2008.